Three-dimensional geometric morphometric analysis of the first metacarpal distal articular surface in humans, great apes and fossil hominins

Lorenzo Galletta[a], Nicholas B. Stephens[b], Ameline Bardo[c], Tracy L. Kivell[c,d,e], Damiano Marchi[f,e*]

[a] *Centre for Integrative Ecology, Deakin University, 75 Pigdons Road, Waurn Ponds, 3216, VIC, Australia*

[b] *Department of Anthropology, The Pennsylvania State University, University Park, PA 1680, USA*

[c] *Animal Postcranial Evolution Lab, Skeletal Biology Research Centre, School of Anthropology and Conservation, University of Kent, Canterbury, CT2 7NR, UK*

[d] *Department of Human Evolution, Max Planck Institute for Evolutionary Anthropology, Deutscher Platz 6, Leipzig, 04103, Germany*

[e] *Evolutionary Studies Institute and Centre for Excellence in PalaeoSciences, University of the Witwatersrand, Private Bag 3, Wits 2050, South Africa*

[f] *Department of Biology, University of Pisa, Via Derna 1, Pisa, 56126, Italy*

* Corresponding author.

E-mail address: damiano.marchi@unipi.it (D. Marchi).

Keywords: Manipulation; *Homo naledi; Homo neanderthalensis*; *Australopithecus africanus*; *Australopithecus afarensis*; *Paranthropus robustus*

Three-dimensional geometric morphometric analysis of the first metacarpal distal articular surface in humans, great apes and fossil hominins

Abstract

Understanding the manual abilities of fossil hominins has been a focus of palaeoanthropological research for decades. Of interest are the morphological characteristics of the thumb due to its fundamental role in manipulation, particularly that of the trapeziometacarpal joint. Considerably less attention has been given to the thumb metacarpophalangeal (MCP) joint, which plays a role in stabilizing the thumb during forceful grasps and precision pinching. In this study we use a three-dimensional geometric morphometric approach to quantify the shape of the first metacarpal head in extant hominids (*Homo*, *Pan*, *Gorilla* and *Pongo*) and six fossil hominin species (*Homo neanderthalensis* Tabun C1 and La Chappelle-aux-Saints, *Homo naledi* U.W. 101-1282, *Australopithecus sediba* MH2, *Paranthropus robustus*/early *Homo* SK84, *Australopithecus africanus* StW 418, *Australopithecus afarensis* A.L. 333w-39), with the aims of identifying shapes that may be correlated with human-like forceful opposition and determining if similar morphologies are present in fossil hominins. Results show that humans differ from extant great apes by having a distally flatter articular surface, larger epicondyle surface area, and a larger radial palmar condyle. We suggest that this suite of features is correlated with a lower range of motion at the MCP joint, which would enhance the thumbs ability to resist the elevated loads associated with the forceful precision grips typical of humans. Great ape genera are each differentiated by distinctive morphological features, each of which is consistently correlated with the predicted biomechanical demands of their particular locomotor and/or manipulatory habits. Neanderthals and U.W. 101-1282 fall within the modern human range of variation, StW 418, SK 84 and U.W. 88-119 fall in between humans and great apes, and A.L. 333w-39 falls within *Pan* variation. These results agree with those of traditional linear analyses while providing a more comprehensive quantitative basis from which to interpret the hand functional morphology of extinct hominins.

Introduction

The highly dexterous human hand is unparalleled among animals, particularly the human ability to generate forceful opposition between the thumb and fingers during object manipulation. Within paleoanthropology, considerable effort has been directed towards understanding the evolution of the human hand, with a primary focus being the relationship between stone tools and the tool-making capacities that can be inferred from fossil hominin hand remains (Midlo, 1934; Napier, 1956, 1960; Tuttle, 1967, 1969, 1981; Marzke and Shackley, 1986; Christel, 1993; Preuschoft and Chivers, 1993; Marzke and Wullstein, 1996; Marzke and Marzke, 2000; Tocheri et al., 2008; Rolian et al., 2011; Kivell et al., 2016). Traditionally, human manipulative performance is considered to be superior to that of extant great apes, with fine motor control, forceful precision grips, and oblique power 'squeeze' grips being cited as unique aspects of human hand-use (Napier, 1956; Marzke and Shackley, 1986; Marzke and Wullstein, 1996; Marzke, 1997). Great apes have a short, gracile thumb and long fingers, which are thought to reflect selective pressures of arboreal locomotion (Napier, 1960; Jouffroy et al., 1993; Patel and Maiolino, 2016). In contrast, the human thumb is distinct in being long relative to the length of the fingers, more mobile and robust, with powerful musculature and an expanded apical tuft that, along with a suite of other morphological features of the hand, are argued to facilitate forceful and dexterous manipulation associated with tool-related behaviors (e.g., Napier, 1956, 1960; Marzke, 1997; Susman, 1998; Young, 2003).

Great apes do not regularly load their thumb during terrestrial locomotion (e.g., Tuttle, 1967; Wunderlich and Jungers, 2009; Matarazzo, 2013), apart from modified forms of fist-walking in *Pongo* (Tuttle, 1967). The thumb is important during power grasping of arboreal substrates, particularly during vertical climbing (Alexander, 1994; Marzke and Wullstein, 1996; Neufuss et al., 2017), although it is not yet completely understood how thumb (and hand) postures might vary across great apes during arboreal locomotion, given the differences in intrinsic hand proportions (Almécija et al., 2015). Although all great apes engage in arboreal locomotor behaviors, the types of locomotion and frequency of each vary substantially across species, with *Gorilla* generally

54 considered to be the least arboreal and *Pongo* the most (e.g., Hunt, 1991; Thorpe and Crompton,
55 2006; Crompton et al., 2010). However, the degree of arboreality can vary between species or even
56 between populations of the same species. For example, mountain gorillas (*Gorilla beringei*) are
57 more terrestrial than lowland gorillas (*Gorilla gorilla*), with females that may be as arboreal as
58 chimpanzees in the same localities (Remis, 1995, 1999; Doran, 1996, 1997; Dunn et al., 2014;
59 Knigge et al., 2015). Among western chimpanzee (*Pan troglodytes verus*) populations, those living
60 in the savanna of Fongoli, Senegal are more terrestrial than chimpanzees living in the forests of Taï
61 National Park, Ivory Coast (Doran, 1992; Pruetz et al. 2009).
62 During manipulation, *Pongo* uses its thumb mainly for gripping small objects (Napier, 1960;
63 Tuttle and Rogers, 1966; Christel, 1993). When manipulating larger objects, orangutans incorporate
64 the mouth or use power grips predominantly involving the fingers, while the thumb, which is
65 extremely reduced compared to the other fingers (Tuttle and Rogers, 1966; Almécija et al., 2015),
66 appears not to provide a forceful contribution to the grip (Napier, 1960; Tuttle, 1969; Pouydebat et
67 al., 2011). In contrast, both *Gorilla* and *Pan* have been documented using hand grips in which the
68 thumb is maintained in secure contact with the object during the grip (e.g., Tuttle, 1969; Byrne et al,
69 2001), with seemingly forceful manipulative actions (Marzke et al., 2015; Neufuss et al., 2018).
70 Among great apes, *Pan* most often engages in tool use in the wild and, in some cases its
71 survival depends on tool use (Napier, 1960; Tuttle, 1969; Boesch and Boesch, 1990, 1993; Jones-
72 Engel and Bard, 1996; Marzke, 1997; Marzke and Marzke, 2000; Crast et al., 2009; Marzke et al.,
73 2015). *Pan* has a relatively limited radioulnar range of motion at the thumb metacarpophalangeal
74 (MCP) joint (12°), more similar to that of humans (10°) than the range of motion in other apes (23°
75 in *Gorilla*, 36° in *Pongo*; Napier, 1960; Tuttle, 1969). Although grip force in chimpanzees has
76 never been empirically measured and they have not been observed to engage in forceful precision
77 grip (Torigoe, 1985; Boesch and Boesch, 1990, 1993; Jones-Engel and Bard, 1996; Pouydebat et al.,
78 2011; Marzke et al., 2015), they do use their thumb frequently during object manipulation, and
79 importantly during 'high force' (as defined by Marzke et al., 2015) V-pocket grips in which the

80 object is grasped in the web between the full thumb and side of the index finger. This grip is often
81 used when grasping large fruits and resisting the pull of the teeth, focusing stresses on the thumb
82 (Marzke et al., 2015), and particularly the MCP joint. Furthermore, *Pan* uses the thumb when
83 grasping arboreal substrates during vertical climbing (Neufuss et al., 2017), in which substrate
84 reaction forces on the forelimb, although not yet measured in *Pan*, are high in other primates
85 (Hirasaki et al., 1993; Hanna et al., 2017; but see Samuel et al., 2018).
86 Like other great apes, *Gorilla* (both mountain and lowland gorillas) has not been observed to
87 use (what appear to be) forceful precision grips (captive *Gorilla gorilla* Parker et al., 1999; wild *G.*
88 *gorilla* Breuer et al., 2005; wild *Gorilla beringei* Grueter et al., 2013). However, mountain gorillas
89 have been observed to frequently use their thumb during food processing (Byrne et al., 2001) where
90 the base of the thumb is used as a fulcrum (Neufuss et al., 2018), and lowland gorillas have been
91 documented to use the thumb particularly during forceful food processing (Marzke, 2006). Indeed,
92 *Gorilla* also shows the highest degree of dorsopalmar and radioulnar curvature in
93 trapeziometacarpal (TMC) joint compared with other great apes, which has been argued to provide
94 greater stability at this joint (*G. beringei*, Marzke et al., 2010; *G. gorilla*, Marchi et al., 2017a).
95 Furthermore, mountain gorillas also use their thumb in vertical climbing and use opposed-thumb
96 postures more often than chimpanzees (Neufuss et al., 2017). In addition, when mountain gorillas
97 descended lianas, the downward pull of the body appears to be resisted mainly by the fingers, while
98 the thenar region of the palm and the proximal phalanx of the thumb counterstabilize the grip
99 (Neufuss et al., 2017).
100 There are several examples of nearly complete and associated hominin hand skeletons,
101 including *Homo neanderthalensis* (Heim, 1982; Trinkaus, 1983; Arensburg et al., 1985),
102 *Australopithecus* sp. (or *Australopithecus prometheus*) (Clarke, 1999, 2013), *Ardipithecus ramidus*
103 (Lovejoy et al., 2009), *Australopithecus sediba* (Berger et al., 2010; Kivell et al. 2011), and *Homo*
104 *naledi* (Berger et al., 2015; Kivell et al., 2015). However, it is more often the case that our
105 understanding of hominin manipulative behavior is based on the functional inferences derived from

isolated and/or unassociated fossil hand remains (e.g., Marzke, 1983; Green and Gordon, 2008; Ward et al., 2013; Domínguez-Rodrigo et al., 2015; Lorenzo et al., 2015; Stratford et al., 2016). As a result, many studies have been devoted to identifying behavioral correlates in human and great ape hand bones that, when identified on fossil hominin hand remains, have allowed inferences to be drawn about the manual behaviors of extinct taxa (Susman, 1979; Tocheri et al., 2005; Lazenby et al., 2008; Matsuura et al., 2010; Almécija et al., 2015; Skinner et al., 2015; Marchi et al., 2017a). In particular, because of the distinctiveness of the human thumb, many studies have investigated the relationship between thumb morphology and manipulative abilities with the aim of identifying features that could be used to infer manipulative abilities of fossil hominins (Napier, 1960; Tuttle, 1969; Rose, 1992; Marzke, 1997, 2013; Marzke and Marzke, 2000; Tocheri et al., 2008; Rolian et al., 2011; Diogo et al., 2012; Shigematsu et al., 2014; Skinner et al., 2015; Marchi et al., 2017a).

The high degree of mobility[1] typical of the human thumb stems in part from the morphology of the TMC joint, which is considered particularly important for manipulation (Napier, 1955; Marzke, 1997; Marzke et al., 2010). Because of this, there have been extensive studies focusing on the functional morphology of the TMC joint (Haines, 1944; Napier, 1955, 1956; Lewis, 1977; Trinkaus, 1989; Rafferty, 1990; Rose, 1992; Marzke, 1997, 2013, Tocheri et al., 2003, 2005; Niewoehner, 2005; Marzke et al., 2010; Marchi et al., 2017a). However, the thumb also comprises the first MCP joint and the interphalangeal (IP) joint, all of which work in concert for effective opposition with the fingers (Imaeda et al., 1992; Li and Tang, 2007). For example, during opposition to the base of the fifth digit, the joints are highly coordinated in flexion, such that, on average, the human TMC joint flexes 50.7°, the MCP joint flexes 41.6° and the IP joint flexes 44.1° (Li and Tang, 2007). Most research on MCP or IP joints of the thumb date to the past century and are often only qualitative assessments (Napier, 1956, 1960; Tuttle, 1969; Aubriot, 1981; Barmakian, 1992; Imaeda et al., 1992). For example, Napier (1960) described the MCP joint as less mobile in

[1] The terms ‘mobility’ and ‘stability’ refer here respectively to joints with a high or low range of motion in all planes (Hamrick, 1996).

130 humans compared to that of great apes. This difference is likely due, at least in part, to the shape of
131 the first metacarpal (MC1) head, which in humans is relatively flat. This flat articulation makes the
132 joint function more like a hinge joint in the flexion-extension plane (Napier, 1960), mainly because
133 of the collateral ligaments that tighten during flexion (Imaeda et al., 1992). In great apes the MC1
134 head surface is more rounded, allowing for higher ranges of motion in the sagittal and radioulnar
135 planes (Napier, 1960). This variation in the MCP joint motion is likely a consequence of the
136 function of the thumb overall. For example, while the human (as well as apes) TMC joint provides
137 high mobility, the human (unlike apes) MCP joint hard and soft tissue morphology provides
138 stability to allow a firm grasp during forceful grips (Barmakian, 1992). However, the lack of
139 quantitative studies, particularly those using 3D methodologies, on thumb joints other than the
140 TMC joint represents a gap in our knowledge that is necessary for fully understanding variation in
141 thumb function in extant and extinct species.
142 In this study we perform a quantitative assessment of the shape of the MC1 head using
143 three-dimensional geometric morphometrics (3DGM) in modern humans (*Homo sapiens*) and
144 extant great ape genera (*Pan*, *Gorilla* and *Pongo*; see Table 1) to provide more informed functional
145 interpretations of fossil hominin morphology. We also include a comparative analysis of several
146 fossil hominin specimens from *H. neanderthalensis*, *H. naledi*, *Paranthropus robustus*/early *Homo*,
147 *A. sediba, A. africanus,* and *Australopithecus afarensis* (Table 1) that preserve a complete MC1
148 head with the aim of further elucidating their potential manipulative abilities.
149 *Homo neanderthalensis* is considered to be the closest relative of modern humans (Endicott
150 et al., 2010) and though many behavioral differences between the two species are acknowledged,
151 morphological and archaeological evidence show that Neanderthals were adept and committed tool
152 users (Bordes, 1961; Lieberman and Shea, 1994; Shea, 2003; Conard and Richter, 2011; Douka and
153 Spinapolice, 2012; Turq et al., 2013; Kuhn, 2014; Karakostis et al., 2018). Neanderthals have
154 different internal thumb proportions (the distal phalanx is relatively longer than the proximal
155 phalanx), and relatively broader joints compared with modern humans, which may affect thumb

function and range of motion (Trinkaus and Villemeur, 1991; Niewoehner, 2006). However, there is no strong evidence indicating that Neanderthals were less dexterous than modern humans (Trinkaus and Villemeur, 1991; Churchill, 2001; Niewoehner et al., 2003; Niewoehner, 2006).

Homo naledi is a recently discovered new species in South Africa (Berger et al., 2015) dated to between 236 and 335 ka (Dirks et al., 2017). Despite its relatively recent age, *H. naledi* shows several primitive traits in the upper and lower limb (Harcourt-Smith et al., 2015; Kivell et al., 2015; Feuerriegel et al., 2017; Marchi et al., 2017b; Williams et al., 2017). A relatively complete hand skeleton (Hand 1) of *H. naledi* has been recovered, along with numerous other hand bones representing at least six adults and two immature individuals (Berger et al., 2015; Kivell et al., 2015). The *H. naledi* hand skeleton combines Neanderthal- and modern human-like features of the wrist and palm that are typically considered adaptations to committed, forceful tool use, with remarkably curved phalanges that suggest a functionally significant degree of climbing or arboreality (Kivell et al., 2015). Among the *H. naledi* remains, there are seven MC1s, although only one preserves a complete distal end (U.W. 101-1282). The preserved morphology in all of the MC1s is generally consistent, having a relatively flat, asymmetrical distal articular surface with a large radial palmar condyle, similar to that of modern humans (Bojsen-Møller, 1976; Aubriot, 1981; Barmakian, 1992), a comparatively small proximal articulation for the trapezium, and well-developed entheses in the distal half of the shaft (Kivell et al., 2015).

Australopiths are generally characterized by adaptations in the lower limb associated with bipedalism (McHenry, 1986; Ward, 2002; Harcourt-Smith and Aiello, 2004). On the other hand, features of the upper limb, such as a relatively long forearm, long and moderately curved manual phalanges in the hand and a cranially-oriented shoulder are related with arboreal behavior (Stern, 2000; Ward, 2002). Concerning the hand, australopith (including *Paranthropus*) MC1 morphology is quite variable, with some being relatively gracile (*A. afarensis, A. africanus* and *A. sediba*) while others being more similar to humans in their robusticity (e.g., SK 84 and SKX 5020 from Swartkrans attributed to either *P. robustus* or early *Homo*; Bush et al., 1982; Susman, 1994; Green

and Gordon, 2008; Kivell et al., 2011). As a result of this hand morphology, australopiths have traditionally been considered unable to perform the full suite of pad-to-pad forceful precision grips typical of humans, but to be more dexterous than extant great apes and capable of making extensive use of natural tools (Marzke and Shackley, 1986; Susman, 1994; Marzke, 1983, 1997; Susman, 1998; Rolian and Gordon, 2013; but see Ricklan, 1987, 1990). However, the recent recovery of more complete hand skeletons (Kivell et al., 2011), new statistical analyses (Alba et al. 2003; Almécija and Alba, 2014) , and analyses of internal bone structure (Skinner et al., 2015) have suggested that australopith hand morphology is compatible with more human-like manipulative skills and the making and utilization of stone tools. This functional interpretation is also compatible with archaeological evidence of percussion and cut-marks at 3.4 Ma (McPherron et al., 2010) and the Lomekwi stone tools at 3.3 Ma (Harmand et al., 2015), both considered to be associated with australopiths.

Australopithecus sediba is a recently discovered australopith species of South Africa, dated to 1.98 Ma (Berger et al., 2010; Pickering et al., 2011). Compared to other australopiths and *Homo*, *A. sediba* possesses a longer thumb relative to short fingers, which is a key feature thought to be compatible with human-like precision grip abilities and potentially stone tool production (Kivell et al., 2011). However, stone tools have yet to be found in association with the *A. sediba* fossils at Malapa (Kivell et al., 2011). A 3DGM analysis of the proximal MC1 articular surface found that *A. africanus* (StW 418) and *P. robustus*/early *Homo* (SK 84) were more ape-like than human-like (Marchi et al., 2017a), and may not have been able to perform the full range of abduction-adduction movements that are associated with stone tool-making and use in humans (Marzke, 1997, 2006). As such, Marchi et al. (2017a) suggested that *A. africanus* and SK 84 may have been making and using stone tools in a manner different from that of later *Homo* and modern humans. Thus, a greater understanding of the thumb MCP joint morphology may provide further insight into the manipulative abilities of australopiths.

3DGM methods have been recently applied to address functional morphological questions in paleoanthropology (e.g., De Groote, 2011; Arias-Martorell et al., 2012; Almécija et al., 2013; Rein et al., 2017; Fernández et al., 2018), including the proximal MC1 (Marchi et al., 2017a), but has not yet, to our knowledge, been used to quantify the shape of the distal MC1. Based on previous literature about thumb morphology and (inferred) function, we will test the following two hypotheses:

(a) We hypothesize that the shape of MC1 head will significantly differ between modern humans and great apes, reflecting a flatter distal articular surface for greater MCP joint stability in humans (Napier, 1960). Moreover, because of the observed differences in hand use during locomotion, and the different degree of tool-use in the wild by extant great apes, we predict that there will be differences among the great ape distal articular MC1 shape. In particular, we predict that *Pan* and *Gorilla* will show greater similarity with humans than *Pongo* due to the observed use of hand grips in *Pan* and *Gorilla* in which the thumb is maintained in secure contact with the object during (what appear to be) forceful manipulative actions (Tuttle, 1969; Byrne et al, 2001; Marzke et al., 2015; Neufuss et al., 2018), which have not been documented in *Pongo*.

(b) Given the inferred manipulative abilities of australopiths, *H. naledi* and Neanderthals, we hypothesize that all fossil hominin specimens will have an MC1 head shape that is more similar to that of humans than to great apes. However, within this context, we predict that Neanderthals will be most similar to modern humans, based on known overall similarities in hand morphology shared between Neanderthals and humans (e.g., Trinkaus, 1983; Niewoehner, 2006), while australopiths and *H. naledi* will show more subtle morphological differences from humans given their earlier age (2–3 Ma) and/or their more gracile (e.g., *A. afarensis*, *A. sediba*) or distinct (i.e., *H. naledi*) MC1 morphology.

Materials and methods

Studied sample

The extant sample used in this study includes MC1s of recent *H. sapiens* (*n* = 24), *Pan troglodytes* (*n* = 25), *Gorilla gorilla* (*n* = 23), *Gorilla beringei* (*n* = 6), *Pongo pygmaeus* (*n* = 32) and *Pongo abelii* (*n* = 5). The fossil sample includes the left MC1 from *A. africanus* StW 418, *H. neanderthalensis* Tabun C1 and *H. naledi* U.W. 101-1282, and the right MC1 from *H. neanderthalensis* La Chapelle-aux-Saints, *A. sediba* MH2 U.W. 88-119, *P. robustus*/early *Homo* SK 84 and *A. afarensis* A.L. 333w-39 (Table 1). The recent *H. sapiens* sample consisted of 17 Medieval (7th C. AD) specimens from a German necropolis (Neuburg, Donau; Marchi, 2005), two specimens from the collection established by Georges Olivier in the 1950s at the Musée de l'Homme in Paris, which consists of unclaimed bodies from Paris hospitals, and five hunter-gatherers specimens from Tierra del Fuego from the first half of the 19th century (Tafuri et al., 2017) curated at the Anthropological Collection of the University of Florence (Italy). For each individual the left MC1 was used and, when not available, the right MC1 was mirrored. Only adult individuals, based on fully-fused epiphyses of all the associated postcranial bones available, were included in the study. Individuals with signs of pathological alterations in the postcranial skeleton were excluded from this study. Due to the small sample size of the *P. abelii*, and their similar hand morphology (Midlo, 1934; Napier, 1960; Tuttle, 1969), *P. abelii* and *P. pygmaeus* were pooled and only genus level differences were investigated in this study.

Three-dimensional surface meshes of the MC1s used in this study where obtained using three methods: computed tomographic (CT) scanning, laser surface scanning, and photogrammetry. Medical CT scans of part of the extant sample were performed at the Munich Institute for Radiology Ludwig Maximilian University (Munich, Germany) on a GE Discovery CT750 HD medical CT scanner (slice thickness 0.625 mm, slice increment 0.3 mm, voltage 120 kV, X-ray tube current 99 mA, reconstructing algorithm bone, pixel size 460 μm), and at the University Hospital of Zurich (Zurich, Switzerland) on a Siemens Somatom Definition Flash (slice thickness 0.6 mm, slice increment 0.3 mm, voltage 120 kV, current 19 mA, reconstructing algorithm bone, pixel size 600

μm). The *Pongo* and the *G. beringei* specimens from the Smithsonian National Museum of Natural History (Washington, USA) were scanned on a Siemens Somatom Emotion CT scanner (slice thickness 1 mm, slice increment 0.1 mm, voltage 110 kV, current 70 mA, reconstructing algorithm H50 moderately sharp kernel, pixel size 600 μm). The Fuegian sample was scanned at the Department of Human Evolution, Max Plank Institute for Evolutionary Anthropology (Leipzig, Germany) on a BIR ACTIS 225/300 scanner (voltage 130 kV, current 100–120 μA, pixel size 30 μm). Fossil specimens StW 418, U.W. 101-1282 and U.W. 88-119 were scanned at the Microfocus X-Ray Computed Tomography facility of the University of Witwatersrand (Johannesburg, South Africa) on a Nikon Metrology XTH 225/320 LC (voltage 70 kV, current 120 μA, no filter used, pixel size 30 μm). A.L. 333w-39 was scanned on SkyScan 1173 (voltage 100 kV, current 62 μA, aluminium filter 1.0 mm, pixel size 30 μm). The Tabun C1 MC1 fossil was scanned at the Imaging and Analysis Centre, Natural History Museum (London, UK) using a Nikon Metrology HMX ST 225 (voltage 200 kV, current 200 μA, copper filter 0.25 mm, pixel size 28 μm). Following data acquisition, image stacks were segmented to produce isosurfaces using Avizo 6.3 software (Visualization Sciences Group, Mérignac, France). The U.W. 101-1282 *H. naledi* MC1 has slight erosion to the palmar-ulnar side of the distal epiphysis. Therefore a mesh was reconstructed using Geomagic Wrap (3D Systems) and Stradwin 5.2 (Treece et al., 2013); see Supplementary Online Material (SOM) S1, and SOM Figs. S1 and S2.

The meshes of the extant ape specimens from the Powell Cotton Museum (Birchington, UK) and of the fossil Neanderthal La Chapelle-aux-Saints from the Musée de l'Homme (Paris, France) were obtained using the NextEngine laser scanner (pixel size 125 μm). Twelve scans were taken at different positions on both sides of the bone and then merged using ScanStudio HD PRO software. A surface model of SK 84, housed at the Ditsong National Museum of Natural History, was made using NextEngine laser scanner (pixel size 125 μm). The meshes of the extant humans from the Musée de l'Homme (Paris, France) and *Pongo* specimens from Leiden Naturalis Museum (Leiden, Netherlands) and of the *G. beringei* specimens from the Royal Museum for Central Africa

285 (Tervuren, Belgium) were obtained through photogrammetry using a Nikon D5100 DSLR camera
286 with a resolution of 24 megapixels. The focal length was fixed to 55 mm for all pictures. Fifty
287 pictures were captured on both side of the bone from different viewpoints. For the reconstruction of
288 the 3D models (pixel size 50 μm) the Agisoft PhotoScan© software (Agisoft LLC, St. Petersburg,
289 Russian Federation) was used. Previous papers have shown that the modality used to generate
290 polygon meshes has minor effect on landmark placing (Robinson and Terhune, 2017; Shearer et al.,
291 2017).
292
293 *3D geometric morphometrics*
294 To quantify the MC1 head morphology we followed the method developed by Fernández et al.
295 (2015) for the metatarsal head. The software Landmark Editor 3.0.0.6 (Wiley et al., 2005) was used
296 to apply a 5 × 5 landmarks patch of nine operator-defined fixed landmarks (Table 2) and 16 surface
297 semilandmarks (automatically placed by the software midway among the others; Fig. 1a). The
298 morphologies we aimed to capture with the 3DGM approach are shown and labeled in Figure 1b.
299 Figure 2 presents an example of MC1 head shape for each of the extant species and for the fossil
300 hominins studied here.
301 A generalized Procrustes analysis (GPA; Gower, 1975) was carried out on all landmark
302 coordinates and surface semilandmarks were slid to minimize the Procrustes distance (Rohlf, 2010).
303 A test using the minimized bending energy criterion (Bookstein, 1997; Gunz et al., 2005) returned
304 similar results (not shown here). To quantify shape variation, aligned shape coordinates resulting
305 from the GPA were subject to a principal component analysis (PCA). Analyses of variance
306 (ANOVAs) on scores along principal components (PCs) were used to test for significant differences
307 across extant genera and Tukey HSD tests were used for pairwise post hoc comparisons. Potential
308 differences between the Fuegian human sample and the remainder of the recent human sample, as
309 well as between *G. gorilla* and *G. beringei* were evaluated using a Hotelling's T^2 test for the

multivariate difference of means on PC1–PC4. Scatterplots and box-and-whisker plots were used to graphically represent data distributions.

We tested for an allometric signal in the data by multivariate linear regression of the first four PC scores using a proxy of body size. The best proxy of body size (when real body size of the specimens is not available) is femoral superoinferior diameter (FemSI; Ruff, 2003). However, we had FemSI diameter only for a subsample of our entire sample (humans $n = 13$; *Pan* $n = 6$; *G. gorilla* $n = 14$; *Pongo* $n = 6$). We therefore carried out a multivariate analysis of covariance (MANCOVA) on the scores of PC1–PC4 using the extant species groups as independent categorical variable and (1) natural log-transformed (ln [FemSI]) as a covariate and (2) ln centroid size (CS) as a covariate. Further, a Procrustes regression analysis of shape on size was carried out when considering for phylogeny using the procD.pgls function of the package geomorph in R (Adams and Otárola-Castillo, 2013). An empirical F distribution for statistical testing was obtained by averaging 10,000 random permutations. The tree for the analysis was built using estimated divergence times published on timetree.org (Kumar et al., 2017).

Fossil hominin specimens were evaluated relative to the comparative extant samples by means of a discriminant function analysis (DFA) on the first three PC scores, treating the fossil hominins as unknown. The DFA classifies specimens into a priori-defined groups, which is a useful tool to evaluate relative similarity of the fossil sample to the extant groups, but it does not give any information on the absolute similarity. To explore absolute similarity of the fossil sample on PC1–PC3 scores, we defined mean shapes for every group by averaging landmark coordinates of every landmark. The mean shape was projected into the tangent shape-space and the relative PC values were calculated. The linear distances of every individual of any extant group to the mean shape of that group were calculated for the first three PCs. These distances were tested for normality using the Shapiro-Wilk test and visually using quintile-quintile (Q-Q) plots. Linear distances of every fossil to the mean of every extant group were then calculated. Fossil distance values were compared to the mean and standard deviation of every extant group and the distance values (in standard

deviations) from the mean were calculated. From these values, the values of the upper tail cumulative distribution function corresponding to the distance of the fossils from the mean of every extant group were calculated. Ultimately, these values correspond to the percentage of individuals in an extant group that are more different from the mean of the group itself than the fossil. For example, if the value obtained for a fossil A compared to modern humans is 75%, it means that fossil A is closer to the human mean distance than 75% of humans.

Finally, visual comparison with group distributions using box-and-whisker plots and comparison to group means via number of standard deviations along PCs were performed, with differences considered significant when the fossil specimens were more than 1 standard deviation away from the mean of extant groups, following Marchi et al. (2017a).

Prior to the statistical analysis, one individual of each extant genus was randomly selected and the landmark placing procedure repeated six times (at least three days apart) to assess the repeatability and accuracy of landmark positioning (Proctor, 2010; Fernández et al., 2015). Sets of repeated measures along measures taken on the other individuals of the same genus were subsequently subject to GPA and PCA, as described above. We tested the hypothesis that relative clustering, and therefore lower variance, of repeated measures should verify the repeatability of landmarks (Lockwood et al., 2002; Proctor et al., 2008; Proctor, 2010; Fernández et al., 2015). This was done by assessing heteroscedasticity between the repeated measures and the rest of the genus using a multivariate correspondent of the Levene test (Anderson, 2006) along the first two PCs.

All statistical analyses were performed in the R environment (R Core Team, 2015) using routines of the package geomorph v 3.0.3 (Adams and Otárola-Castillo, 2013). R was also used to create graphical outputs to interpret the results and for visualization purposes using the package rgl v 0.97.0 (Adler et al., 2017).

Results

Allometric analysis

362 The analysis on the scores of PC1–PC4 using the extant species groups as independent
363 categorical variables and (1) ln FemSI as a covariate and (2) ln CS as a covariate gave virtually
364 identical results (SOM Fig. S3; SOM Table S1), validating the use of CS as a proxy of body size.
365 Results of the MANCOVA when using the two different covariates and on different subsample
366 sizes are almost identical, and all indicate that the influence of size on shape is minor when
367 compared to other aspects (SOM Table S2). The phylogenetic comparative analysis returns a
368 nonsignificant *p*-value ($p = 0.06$), showing how size does not influence significantly the shape of
369 the MC1 head when analyzed in a phylogenetic context. Overall, the above analyses suggest that,
370 for the aims of this study, we can exclude size as a significant factor contributing to potential
371 interspecific variation in shape.
372
373 *Repeatability and Accuracy*
374 Graphical output of the repeatability test is shown in SOM Figure S4 and statistical testing
375 results are reported in SOM Table S3. For all taxa, repeated measures in the morphospace were
376 clustered and easily recognizable from the rest of the sample. Statistical testing supports this
377 separation with all tests being significant ($p < 0.05$). Therefore, we conclude that the landmark
378 placement is repeatable for the purposes of this study.
379
380 *PCA, ANOVA and Tukey HSD test*
381 The first four PCs in the PCA account for more than 50% of total variance. PC1 explains 27.2%
382 of total variance, PC2 11.2%, PC3 10.3% and PC4 7.4%. PC5 and beyond are not significant ($p \geq$
383 0.05) and are not discussed further. ANOVA shows that groups are significantly separated along
384 PC1 ($p < 0.001$), PC2 ($p < 0.001$), PC3 ($p < 0.001$) and PC4 ($p < 0.05$). No significant differences
385 are found between the Fuegian sample and the remaining recent human sample, or between *G.*
386 *beringei* and *G. gorilla* (Hotelling's T^2 test results; SOM Table S4), each showing overlapping
387 distributions in both comparisons (SOM Figures S5 and S6). Thus, the two human groups and the

two *Gorilla* genera were pooled in all subsequent analyses, although the Fuegian and *G. beringei* specimens are highlighted in the PCA plots in SOM Figures S7–S9.

Along PC1 and PC2 each genus is significantly different from any other group ($p < 0.05$; Tables 3 and 4). Along PC3, recent humans and *Pongo* are significantly different from *Pan* and *Gorilla* ($p < 0.01$; Table 5), while no significant difference is present between African great apes. Along PC4 great overlap among extant species is present (SOM Figs. S10 and S11). The only significant difference is between *Pan* and *Gorilla* ($p < 0.05$; SOM Table S5).

A bivariate scatterplot of PC1 against PC2 (Fig. 3) successfully separates humans from all great apes with only slight overlap with the *Gorilla* morphospace. Great ape groups partially overlap in the morphospace, yet each of the three genera shows a well-defined tendency: *Pongo* morphospace occupies only the two left quadrants of the morphospace, being characterized by negative PC1 scores; *Pan* occupies prevalently the left upper quadrant of the morphospace and *Gorilla* the central part of the morphospace. As for the fossil hominins, Neanderthals (Tabun C1 and La Chapelle-aux-Saints), U.W.101-1282, SK 84 and StW 418 fall within the human morphospace, although SK 84 and StW 418 fall in the region of overlap between the recent human and *Gorilla* morphospaces. U.W. 88-119 falls within the *Pan* morphospace and close to the *Gorilla* morphospace and A.L. 333w-39 falls within the *Pan* morphospace.

A bivariate scatterplot of PC1 against PC3 (Fig. 4) mainly divides *Gorilla* (along PC3) and humans (along PC1) from the other groups, although there is substantial overlap among the great apes. Humans fall mostly within the upper right quadrant of the morphospace and only marginally overlap with *Pan* and *Gorilla*. Only the Neanderthal specimens (Tabun C1 and La Chapelle-aux-Saints) and U.W. 101-1282 fall within the modern human morphospace. A.L. 333w-39 falls in the overlapping region of *Pan* and *Pongo,* while StW 418, SK 84 and U.W. 88-119 fall in the upper right quadrant outside the morphospace of any extant group.

412 A bivariate scatterplot of PC1 against PC4 shows high overlap among extant groups not
413 being useful for fossil determination. We therefore discuss PC4 results in SOM S2 and show them
414 in SOM Figures 9 and 10 and SOM Table S5, but do not discuss them further in the main text.
415
416 *PC1 shape and groupings*
417 The shape variations described by the PC1 are most informative in distinguishing humans from
418 the great apes (Figs. 3 and 5; Table 3). The positive side of the PC1 axis is occupied primarily by
419 modern humans and describes a shape of the distal articular MC1 surface that is relatively flatter
420 and radioulnarly wide. Additionally, the radial palmar condyle is much larger than the ulnar palmar
421 one, and both the radial and ulnar epicondyles are slightly enlarged (Fig. 5). The negative side of
422 PC1 is occupied primarily by *Pongo* and secondarily by *Pan*, even though overlap with *Gorilla*
423 occurs. The negative side of PC1 describes a shape with an articular surface radioulnarly narrow
424 and dome-like. The radial palmar condyle is small, almost equal in size to the ulnar palmar condyle,
425 and the radial and ulnar epicondyles are slightly smaller as well (Fig. 5). Regarding the fossil
426 specimens, La Chapelle-aux-Saints, Tabun C1 and U.W. 101-1282 fall in the interquartile range of
427 humans. StW 418 and SK 84 fall in the lower quartile range of humans, with SK 84 falling also in
428 the upper interquartile of *Gorilla* (Fig. 5). Neanderthals and U.W. 101-1282 are the only fossils
429 within 1 standard deviation (SD) of humans mean (Table 6). A.L. 333w-39 falls in the interquartile
430 range of *Pan* and *Pongo* and is within 1 SD of their mean (Fig. 5; Table 6).
431
432 *PC2 shape and groupings*
433 The shape differences described by PC2 are most informative in separating *Pan* from the other
434 extant groups (Fig. 6; Table 4). The positive side of the PC2 axis is occupied primarily by the *Pan*
435 group and secondarily by the modern human group and describes a shape with a relatively straight
436 articular ridge on the palmar side (defined as palmar articular ridge; Fig. 1b), an articular surface
437 that extends further onto the dorsal surface and is radioulnarly flatter, a quadrate contour of the

438 articular surface, and relatively small epicondyles. In addition, the radial palmar condyle is
439 relatively radioulnarly narrow and projects palmarly. The negative aspect of PC2 axis, occupied
440 mostly by *Gorilla* and *Pongo*, describes a shape with a more pronounced curvature of the palmar
441 articular ridge, a radial palmar condyle projecting more radially, larger epicondyles, and a more
442 curved articular surface in the radioulnar plane. Box-and-whisker plots show that all fossils with the
443 exception of A.L. 333w-39 fall in the human interquartile range (and variably in the *Pan* and *Pongo*
444 ranges) and outside the *Gorilla* range. Tabun C1 and U.W. 101-1281 are within 1 SD of humans
445 mean (Fig. 6; Table 6). However, La Chapelle aux Saints falls within 1 SD of *Gorilla* and *Pongo*.
446 SK 84 and StW 418 fall in the lower quartile range of humans and within 1 SD from their mean and
447 within 1 SD of *Pongo* means (Fig. 6; Table 6). A.L. 333w-39 falls neatly outside the human
448 distribution in the upper quartile range of *Pan* and within 1 SD from its mean (Fig. 6; Table 6).
449
450 *PC3 shape and groupings*
451 The shape variability described by the PC3 are most informative in distinguishing African great
452 apes from recent humans and *Pongo* (Fig. 7; Table 5). The positive portion of PC3, occupied by
453 humans and *Pongo*, represents slightly larger radial palmar condyles and radioulnarly flatter
454 articular surface. The negative portion of PC3, occupied by *Gorilla* and *Pan*, represents relatively
455 larger epicondyles. U.W. 101-1282, La Chapelle aux Saints and A.L. 333w-39 fall variably within
456 the upper range of African great apes and are almost always (apart from A.L. 333w-39) within 1 SD
457 of the two species mean (Fig. 7; Table 6). Tabun C1 falls in the interquartile range of recent humans
458 and *Pongo* distributions, and is within 1 SD of the two species mean. StW 418, SK 84 and U.W. 88-
459 119 fall above the range of all extant groups and are almost always (apart from SK 84) more than 1
460 SD from their means (Fig. 7; Table 6).
461
462 *DFA and linear distance of fossils*

Results of the DFA and of the distance in tangent space of fossil specimens from group specimens are reported in Table 7. Fossil specimens U.W. 101-1282, Tabun C1, StW 418, La Chapelle-aux-Saints and SK 84, are classified as humans with 99.9%, 97.5%, 88.6%, 76.6% and 59.1% of probability in the DFA, respectively. U.W. 88-119 is classified as *Pongo* with 38.4% probability, as *Pan* with 32.0% of probability, and as recent human with 29.7% of probability. A.L. 333w-39 is classified as *Pan* with 97.8% of probability (Table 7).

Results of the Shapiro-Wilk tests are reported in Table 8 and Q-Q plots are shown in SOM Figure S12. All distributions were not significantly deviating from normality. Thus, for each extant group we assumed a normal distribution for the distances of each individual within the group from the mean shape of the group itself. Fossils distances (in SD from the mean of the distance of each individual of the group from the group mean) are reported in Table 9 and graphically represented in SOM Figure S13. Results agree with the output of the DFA. Tabun C1, La Chapelle-aux-Saints and U.W. 101-1282 are closer to the human mean than 77.2%, 43.9%, and 53.7% of recent humans, respectively, corroborating the similarity of their shape to that of humans found in the DFA classification. StW 418 and SK 84, despite being more similar to humans than to other groups in the DFA classification, bear a low absolute similarity, being closer to the human mean than just 5.46% and 5.01% of humans, respectively. A.L. 333w-39 is closer to the *Pan* mean than 75.7% of *Pan* individuals. U.W. 88-119 is far from every extant group mean, being closer to the mean than less than 0.1% of every group's individuals. Thus, U.W. 88-119 is distinct among our fossil sample in being outside of the morphospace range of every extant group.

Discussion

The aim of this study was to quantify the shape variability of the distal articular surface of the MC1 using 3DGM methodology to provide more informed functional interpretations of fossil hominin morphology. We hypothesized that the shape of human MC1 head will be significantly different from that of great apes and predicted that, among great apes, *Pan* and *Gorilla* would be

more similar to each other than to *Pongo*. Results from our analyses provide support to the hypothesized distinct morphology between recent humans and great apes and among African and Asian great apes. Our second hypothesis was that fossil hominins would have MC1 head shape that is more similar to humans than to that of great apes, but that there would be some morphological variation among the fossil specimens. Our results provide only partial support for this hypothesis. Overall, however, our results demonstrate the utility of 3DGM to quantify, often subtle, differences in MC1 head morphology and provide further insight into the function of the thumb in extant hominids and fossil hominins.

Human and great apes MC1 head shape

Results showed that the MC1 head shape of recent humans is significantly different from that of great apes, supporting our first hypothesis. The morphology of human MC1 head is characterized by a flattened and radioulnarly enlarged articular surface (as already observed by Susman, 1994), relatively large epicondyles, and a radial palmar condyle that is larger and more palmarly projecting than the ulnar one (see Fig. 3). Moreover, both palmar condyles tend to be less proximally positioned in humans than in great apes. All these morphological traits are consistent with the proposed stabilization role that the MCP joint has in humans compared to apes for limiting thumb movement during forceful power and precision gripping, which counterbalances the mobility of the TMC joint (Aubriot, 1981; Barmakian, 1992). The broader and flatter MC1 distal articular surface limits dorsopalmar motion and prevents almost all radioulnar motion (Aubriot, 1981; Barmakian, 1992; Imaeda et al., 1992).

The relatively large size of radial and ulnar epicondyles in humans is correlated with a lower range of motion at the MCP joint. Collateral ligaments originate from the epicondyles and insert at the base of the proximal phalanx. When the thumb is flexed, the collateral ligaments tighten to limit radioulnar motion of the proximal phalanx, emphasizing the primarily hinge-like flexion-extension motion of the MCP joint in humans (Aubriot, 1981; Barmakian, 1992; Imaeda et al., 1992). We

515 hypothesize that bigger epicondyles in humans allow for a larger attachment area of ligaments that
516 are therefore potentially stronger and able to help stabilize the MCP joint during the high forces that
517 are experienced by the thumb during manipulation. Further studies are necessary to test this
518 hypothesis, including anatomical dissections on nonhuman apes to evaluate the hypothesized
519 relationship between epicondyle and ligament size.

520 The larger palmar radial condyle observed in humans has been related to the conjoint
521 rotation that occurs at the MCP joint during flexion, such that proximal phalanx pronates as it flexes
522 (Bojsen-Møller, 1976; Aubriot, 1981; Barmakian, 1992). It was proposed that the larger palmar
523 radial condyle fits into a depression on the radiopalmar aspect of the proximal phalanx articular
524 surface when the thumb is flexed (Bojsen-Møller, 1976). This joint mechanism should prevent
525 movements in the radioulnar plane providing more overall stability of the joint when subjected to
526 loading. More recent studies, however, showed the inaccuracy of describing articulations as
527 'locking devices' as in Bojsen-Møller (1976) and proposed articular stability is mainly provided by
528 musculature and ligaments (Lovejoy et al., 2001, 2009). Due to the strong discriminatory power of
529 the palmar radial condyle highlighted in the present study, we encourage future kinematic studies to
530 look into this structure to better understand the function of its morphology.

531 In support of our prediction, the analyses show significant differences along single PCs in
532 the morphology of MC1 distal articular surface across great apes. The shape variation we found in
533 the distal MC1 morphology may reflect variation in the frequency and type of locomotion
534 (terrestrial vs. arboreal), variation in the thumb posture during grasping, or both (Tuttle, 1967; Hunt,
535 1991; Alexander, 1994; Marzke and Wullstein, 1996; Thorpe and Crompton, 2006; Wunderlich and
536 Jungers, 2009; Crompton et al., 2010; Almécija et al. 2015; Neufuss et al. 2017, 2018). *Pongo* show
537 a relatively round and domed articular surface, small epicondyles and similarly-sized palmar
538 condyles (see Fig. 2). This morphology is consistent with a high range of motion at the MCP joint
539 documented in *Pongo* during flexion, but particularly hyperextension and radioulnar deviation,
540 which are greater than that of *Pan* and *Gorilla* (Napier, 1960; Tuttle, 1969). Captive studies show

that orangutans use their thumb less during manipulative tasks than other great apes, repositioning tools/food more often with their mouth than with their hands (Christel et al., 1993; Bardo et al., 2017). However, orangutans are able to use pad-to-side precisions grips as other great apes do (Christel, 1993; Pouydebat et al., 2009; Bardo et al., 2017). Among extant hominids, orangutans also have the shortest thumb relative to the fingers among hominids (Schultz, 1930; Napier, 1993; Almécija et al., 2015), which implies greater biomechanical constraints (e.g., muscle force and joint angles) during tool manipulation compared to African great apes (Bardo et al., 2018). The specific MC1 head morphology of *Pongo*, and the fact that it is more ulnary rotated relative to its TMC joint compared to African great apes (Drapeau, 2015), may allow for greater motion of the MCP joint to balance the constraints of a short thumb (Schultz, 1930; Napier, 1993; Almécija et al., 2015) and more limited TMC joint motion (Rafferty, 1990).

The *Pan* MC1 head is characterized by an articular surface that is relatively flat, similar to the morphology found in humans. Yet, in contrast to humans, *Pan* MC1 head bears palmar condyles that are almost equal in size, as well as small dorsal epicondyles. This morphology is described by the overall positive scores along PC2 of *Pan* specimens. Like in humans, a flatter articular surface will limit motion at the MCP joint, particularly in the radioulnar plane, making the joint function more like a hinge joint (Imaeda et al., 1992). This is consistent with quantitative data showing the relatively limited radioulnar range of motion in *Pan* and humans compared to other great apes (Tuttle, 1969). However, the smaller radial and ulnar epicondyles in *Pan* MC1 head are an indication that the MCP joint collateral ligaments are perhaps not as well developed. This morphology suggests that *Pan* MCP joint is less stable than that of humans, and thus less able to sustain high and/or prolonged forces that occur during forceful precision gripping in humans (Domalain et al., 2008). This morphology is consistent with the use of pad-to-side precisions grips in chimpanzees (Marzke and Wullstein, 1996, Marzke et al., 2015), rather than pad-to-pad precisions grip used by humans (Marzke, 1997; Marzke et al., 1992), and the use of more simple in-hand movements compared to humans (Elliot and Connolly, 1984; Crast et al., 2009; Bardo et al.,

2017). Moreover, chimpanzees have been shown to use their thumb in line with the arboreal substrate, rather than wrapping around, during diagonal power grasping (Marzke et al., 1992; Neufuss et al., 2017). Thus, the radioulnarly flat articular surface in the *Pan* MC1 may play a role in stabilizing the MCP joint during arboreal locomotion, as well as manipulation (Tuttle, 1969; Christel, 1993; Marzke et al., 2015).

The *Gorilla* distal MC1 showed particularly large epicondyles, palmar condyles that are equal in size, but rounder articular surface than in humans and *Pan*. The large epicondyles may indicate stronger, well-developed collateral ligaments relative to *Pan* and humans to aid the stabilization of the MCP joint. However, a rounder articular surface and the lack of a large radial palmar condyle suggests that the *Gorilla* distal MC1 morphology is more mobile and perhaps less able to cope with large, sustained forces on the thumb compared to that of humans. Wild mountain gorillas frequently use their thumb for processing food, in particular during forceful food processing (Byrne et al., 2001; Neufuss et al., 2018), and use a variety of thumb positions during arboreal locomotion and food manipulation (Neufuss et al., 2017, 2018). However, both wild mountain gorillas (Neufuss et al., 2018) and captive western lowland gorillas (Bardo et al., 2017), appear to use more adducted thumb during manipulation. Like chimpanzees, captive western lowland gorillas also use simple in-hand movements (Bardo et al., 2017). Although subtle differences in hand proportions (Almécija et al., 2015) and MC1 head breadth (relative to MC1 length; Hamrick and Inouye, 1995) have been documented previously between mountain and lowland gorillas, our analysis did not find any significant difference between these two species in MC1 distal joint shape. The lack of interspecific morphological differences found here may reflect the low sample size (n = 6) of *G. beringei*, or indicate that both *Gorilla* species require a more stable MCP joint relative to *Pan*, regardless of the differences in thumb use observed between them, though evidence is lacking at present to support this hypothesis. Additional studies on both *Gorilla* species are needed to quantitatively describe the MC1 distal joint morphology and its relationship to their respective manual behavior.

593

594 *Fossil hominins MC1 head shape*

595 It is generally accepted that Neanderthals had manipulative abilities similar to those of *H.*
596 *sapiens* (Marzke and Shackley, 1986; Trinkaus and Villemeur, 1991; Niewoehner et al., 1997;
597 Niewoehner, 2000, 2006; Tocheri et al., 2008; Karakostis et al., 2018). Thus, it is not surprising that
598 both Neanderthal specimens included in this study fell within the ranges of recent humans for most
599 of the PCs (Figs. 6-9).

600 Slight differences in the use of power grips over precision grips have been previously
601 inferred from some features of the Neanderthal hand, such as increased mechanical advantage of the
602 flexor muscles acting at the thumb MCP joint, reduced mechanical advantage of muscles crossing
603 the thumb interphalangeal joint (Trinkaus and Villemeur, 1991), general muscular hypertrophy,
604 other muscles mechanical advantages (for a review, see Niewoehner, 2006). In a comparative
605 analysis of hand morphology between Neanderthals and recent humans, Niewoehner (2006)
606 suggested that the change in tool materials and use that occurred during the Upper Paleolithic may
607 have triggered a change in bone morphology towards a more human-like condition, including
608 increased abilities in precision handling. On the other hand, a recent study based on hand entheseal
609 surface areas (Karakostis et al., 2018) challenged the general view that Neanderthals primarily used
610 power grips when making and/or using Mousterian tools and proposed that they performed
611 precision grasping in their daily activities. The results of the present study provide support for a
612 more modern human-like use of the hand by Neanderthals.

613 Along PC3, La Chapelle-aux-Saints scored more than 1 SD lower than the human mean.
614 The lower score along PC3 indicates larger dorsal epicondyles and a slightly rounder articular
615 surface (especially in the radioulnar plane) compared to the average modern humans. This
616 combination of traits moves La Chapelle-aux-Saints near the morphospace of *Gorilla*, as is
617 confirmed by the DFA analysis. However, the analysis of absolute morphological similarity (Table
618 9) shows that La Chapelle aux Saints is closer to the human mean than 43.9% of humans. The La

619 Chapelle-aux-Saints individual shows extensive osteoarthritis of its skeleton (Trinkaus, 1985),
620 which could have biased the 3DGM analysis. However, the MC1 analyzed here did not show any
621 sign of osteoarthritis, and manipulative abilities of the MCP joint should not be hampered by
622 osteoarthritis in other part of the skeleton.
623 Previous studies on the hand of *H. naledi* described its thumb morphology as derived, with
624 well-developed extrinsic and intrinsic musculature, along with Neanderthal/modern human-like
625 morphology to the radial carpometacarpal articulations, which are compatible with forceful
626 precision grip and human-like manipulative abilities (Kivell et al., 2015). Our results support this
627 interpretation, as the shape of the MC1 distal joint of U.W. 101-1282 falls within the range of
628 humans along all PCs. The DFA and the distances in standard deviations from the mean of the
629 modern human sample corroborate this result as U.W. 101-1282 is consistently classified as human
630 and is much closer to humans than it is to great apes. These traits may indicate that *H. naledi*'s
631 thumb MCP joint was adapted to sustain high loads (i.e., radioulnarly flat) but perhaps with less
632 stability compared to recent humans (i.e., smaller epicondyles). Of course, only a single *H. naledi*
633 specimen could be included in the present analysis, and it is possible it does not reflect the average
634 morphological condition of this species. Further, the slight erosion present on the palmar ulnar side
635 of the *H. naledi* MC1 studied here may also influence the analysis. More well-preserved *H. naledi*
636 specimens are needed to better understand if U.W. 101-1282 is representative of the species and a
637 more holistic analyses of the entire MC1 shape will provide much-needed insight into how the
638 radioulnarly broad distal articulation functions in concert with such a small TMC joint.
639 Earlier research of South African australopith MC1 specimens U.W. 88-119, SK 84 and
640 StW 418 have interpreted the morphology as being consistent with enhanced (Green and Gordon,
641 2008) or even human-like manipulative abilities (Kivell et al., 2011; Skinner et al., 2015). The MC1
642 head shape of U.W. 88-119, SK 84 and StW 418 differs slightly from that of humans. The three
643 hominins have an articular surface that is not as curved as in great apes but not as flat as in humans.
644 Similarly, they show larger epicondyles and a larger radial palmar condyle than that of the average

645 great ape, but not as large as in humans. Interestingly, the three fossil hominin specimens fall above
646 the range of the modern humans (and of all the other extant groups) along PC3, indicating a
647 relatively larger radial palmar condyle and radioulnarly flatter articular surface. In the DFA, StW
648 418 and SK 84 are classified primarily as human, while U.W. 88-119 is classified primarily as
649 *Pongo*. However, when analyzing the distances in standard deviations from the mean of the recent
650 human sample, the three South African australopiths are among the most different from humans
651 within our fossil sample (*A. afarensis* excepted; Table 9). Our results therefore indicate that, based
652 on bone shape alone, the MCP joint of South African australopiths may have provided greater
653 stabilization during gripping than that of *Pan*, but less than that of recent humans and Neanderthals.
654 In a recent study, Skinner et al. (2015) proposed a human-like use of the hand in *A. africanus* based
655 on the distribution of trabecular bone within the MC1like that of *H. sapiens* and Neanderthals in
656 StW 418 (and SK 84). As previously observed by Marchi et al. (2017a), while trabecular bone
657 structure may provide additional insight into the actual load to which a bone was subjected during
658 life (but see Judex et al. 2004; Carlson et al., 2008), external bone morphology—and therefore
659 distal MC1 joint shape—can give us useful information about the type and range of movements that
660 were possible at the level of the articulation. The results of the analysis of the shape of the proximal
661 (Marchi et al., 2017a) and distal (present study) articular surface of MC1 indicates that South
662 African australopiths may not have been able to perform the complete range of movements that we
663 associate today with stone tool-making and use (Marzke, 1997, 2006). It is interesting to note that *A.*
664 *sediba* MC1 and SK 84 are not grouped together in any of the analyses performed in this study. The
665 two fossils share a unique morphology, namely a bony beak present palmarly on the head of MC1.
666 Landmark 2 in our landmark setting (Table 2) is placed right at the point of the bony peak to
667 capture this morphology. The reason why such morphology is not recorded in any of the PCs is
668 probably due to the fact that only a minimal variation is explained by this morphology in any of the
669 analyzed PCs. 3DGM is not the best method to classify specimens on the basis of unusual
670 morphologies. If this distinct trait is to be investigated in future studies, we suggest that (1) the

incidence of this trait in modern humans be determined; (2) kinematic studies be performed to determine the possible association of this bony beak with differences in MCP joint movements; and (3) dissections be performed to establish the association of this trait with ligaments/muscles size/insertions.

The MC1 shape of *A. afarensis* A.L. 333w-39 is the most different among our fossil sample from that of recent humans. A.L. 333w-39 has an articular surface that is much more curved radioulnarly than in humans, with smaller epicondyles and a smaller radial palmar condyle that are more similar to those of *Pan* than to humans (Figs. 3,4). The similarity of A.L. 333w-39 to *Pan* is highlighted along all the PCs (Figs. 5–7). Although there is a large sample of *A. afarensis* hand bones from multiple sites (Bush et al., 1982; Ward et al. 2012), few of them are associated to the same individual (Drapeau et al. 2005), making interpretations of hand function challenging. There is debate over the intrinsic hand proportions of *A. afarensis*, which may range from *Gorilla*-like with a relative short thumb (Rolian and Gordon, 2013) to human-like (Alba et al. 2003; Almécija and Alba, 2014), and hold different implications for precision grip ability. Previous morphological studies have suggested *A. afarensis* was capable of at least some forceful precision grips, which would have aided in the manufacture and use of tools (Marzke and Shackley, 1986; Alba et al. 2003), but with potentially limited capacity to use power squeeze grips (Marzke, 1983). However, recent archaeological evidence associated with *A. afarensis* indicates that the hand morphology of these early hominins, at least in East Africa, was capable of using and making stone tools (McPherron et al., 2010; Harmand et al., 2015). Although stone tools have not been found in association with South African australopiths, previous studies conducted on trabecular bone may provide biomechanical evidence of stone tool making capability in *A. africanus* (Skinner et al., 2015). The 3DGM analysis performed here is not suggesting that australopiths were not able to make and use stone tools. What the study of external morphology of MC1 suggests is that, if australopiths were making and using stone tools (as archaeological evidence is suggesting at least in East Africa;

McPherron et al., 2010; Harmand et al., 2015), they were making and/or using them in a different way compared to later *Homo* and modern humans.

A recently published paper on the 3D surface morphology of metatarsal I–V head (Fernanández et al., 2018) provided important insight on the evolution of the hominin forefoot. A further step in the investigation on the evolution of early hominin manipulatory abilities should be the inclusion of all MCs in the analysis. We also need to keep in mind that the MCP joint is constituted not only by the MC1 head but also by the proximal phalanx joint. The inclusion of the proximal articulation of the proximal phalanx, using the protocol already employed for the proximal MC1 joint (Marchi et al., 2017a), will add further information to the understanding of this complex articulation and its evolution in the hominin lineage.

Conclusions

In this study we quantified and compared the shape of the MC1 head in modern humans, chimpanzees, gorillas and orangutans. In this framework, we also quantified the shape of the MC1 head in seven fossil hominins that were (or have been suggested to be) able to produce and use tools: Tabun C1 and La Chapelle-aux-Saints (*H. neanderthalensis*), U.W. 101-1282 (*H. naledi*), U.W. 88-119 (*A. sediba*), SK 84 (*P. robustus*/early *Homo*), StW 418 (*A. africanus*), and A.L. 333w-39 (*A. afarensis*). Our results are in general agreement with previous studies, yet new details can be discerned that can be associated with human manipulatory abilities. We found that the recent human MC1 head is characterized by a distinct suite of traits, including relatively larger epicondyles, asymmetric palmar condyles and a larger, more palmarly-pronounced radial palmar condyle, that can all be related to greater stability of the thumb MCP joint, which is necessary for forceful precision grip. We suggest that the presence of all three morphological features in a fossil hominin is a strong signal for human-like manipulative use of the thumb. Australopiths from both South and East Africa, although displaying MCP joint morphology that was similar in some aspects to recent

humans, did not show all three of morphological features suggesting a reduced manipulative capacity in australopiths when compared to the representatives of the genus *Homo*.

Acknowledgements

The authors are grateful to the following individuals and institutions that provided access to specimens in their care: K. Isler, University of Zurich, Irchel, Switzerland and G. Grupe, University of Munich, Germany, as well as J. Grimm at the University of Munich Institute for Radiology for assistance with medical CT scanning; B. Billings for access to the Raymond A. Dart Collection at the School of Anatomical Sciences, I. Livne at the Powell Cotton Museum, Birchington; D. Grimaud-Hervé, M. Friess, V. Laborde, L. Huet, A. Fort at the MNHN Musée de l'Homme, Paris; P. Kamminga at the Naturalis Biodiversity Center, Leiden; E. Gilissen and W. Wendelen at the Royal Museum for Central Africa, Tervuren; C. Boesch in the Department of Primatology, Max Planck Institute for Evolutionary Anthropology (MPI-EVA); J. Moggi Cecchi and S. Bortoluzzi, University of Florence; F. Mayer and S. Jancke, Museum für Naturkunde – Leibniz Institute for Evolution and Biodiversity Science, Berlin; K. Helgen of the Smithsonian's Division of Mammals and M. Tocheri of the Human Origins Program for the scans of USNM specimens used in this research (http://humanorigins.si.edu/evidence/3D-collection/primate), which were acquired through the generous support of the Smithsonian 2.0 Fund and the Smithsonian's Collections Care and Preservation Fund. We are also grateful to S. Potze and L. Kgasi at the Ditsong National Museum of Natural History for access to SK 84; B. Zipfel and L. Berger for access to fossils StW 418, U.W. 88-119 and U.W. 101-1282 and Kudakwashe Jakata for microCT scanning material at the Evolutionary Studies Institute, University of the Witwatersrand; R. Kruszynski at the Natural History Museum London for access to Tabun C1 and L. Buck for microCT scanning. The access to A.L. 333w-39 was made possible through the support and effort of B. Kimbel, Z. Alemseged, F. Spoor and D. Plotzki (microCT scanning) in collaboration with the National Museum of Ethiopia, and with permission from the Authority for Research and Conservation of the Cultural Heritage,

747 and this research is supported by the Department of Human Evolution, Max Planck Institute for
748 Evolutionary Anthropology, the Institute of Human Origins, Arizona State University, California
749 Academy of Sciences. We thank A. Massolo for helpful discussions concerning the statistical
750 analyses used in this research. Finally, we thank three anonymous reviewers which provided useful
751 comments that improved the manuscript. This research is supported in part by the Department of
752 Biology, University of Pisa (551-60% 2018), the Department of Human Evolution, MPI-EVA
753 (N.B.S., T.L.K.), the Fyssen Foundation (A.B.) and the European Research Council Starting Grant
754 336301 (T.L.K.).

755
756 **Author contributions**

757 D.M. conceived the project. L.G. performed the statistical analyses. D.M., T.L.K., A.B. and N.B.S.
758 provided comparative data. N.B.S. performed the digital correction of the slightly eroded U.W. 101-
759 1282 MC1 head. All authors participated in the interpretation of results. L.G. and D.M. wrote the
760 paper with contributions from all authors.

761
762

763 **References**

Adams, D.C., Otárola-Castillo, E., 2013. Geomorph: an r package for the collection and analysis of geometric morphometric shape data. Methods in Ecology and Evolution 4, 393–399.

Adler, D., Murdoch, D., Nenadic, O., Urbanek, S., Chen, M., Gebhardt, A., Bolker, B., Csardi, G., Strzelecki, A., Senger, A., Eddelbuettel, D., 2017. rgl: 3D visualization using OpenGL, R package. https://CRAN.R-project.org/package=rgl.

Alba, D.M., Moyà-Solà, S, Köhler, M., 2003. Morphological affinities of the *Australopithecus afarensis* hand on the basis of manual proportions and relative thumb length. Journal of Human Evolution 44, 225-254.

Alexander, C.J., 1994. Utilisation of joint movement range in arboreal primates compared with human subjects: an evolutionary frame for primary osteoarthritis. Annals of Rheumatic Diseases 53, 720-725.

Almécija, S., Alba, D.M., 2014. On manual proportions and pad-to-pad precision grasping in *Australopithecus afarensis*. Journal of Human Evolution 73, 88-92.

Almécija, S., Tallman, M., Alba, D.M., Pina, M., Moyà-Solà, S., Jungers, W.L., 2013. The femur of *Orrorin tugenensis* exhibits morphometric affinities with both Miocene apes and later hominins. Nature Communications 4, 2888.

Almécija, S., Orr, C. M., Tocheri, M. W., Patel, B. A., Jungers, W. L., 2015. Exploring phylogenetic and functional signals in complex morphologies: the hamate of extant anthropoids as a test-case study. The Anatomical Record 298, 212–229.

Anderson, M. J., 2006. Distance-based tests for homogeneity of multivariate dispersions. Biometrics 62, 245–253.

Arensburg, B., Bar-Yosef, O., Chech, M., Goldberg, P., Laville, H., Meignen, L., Rak, Y., Tchernov, E., Tillier, A.-M., Vandermeersch, B., 1985. Une sépulture néandertalienne dans la grotte de Kebara (Israël). Comptes Rendus de l'Académie des Sciences Paris 300, 227–230.

Arias-Martorell, J., Patau, J.P., Bello-Hellegouarch, G., Pastor, J.F., Pérez-Pérez, A., 2012. 3D geometric morphometric analysis of the proximal epiphysis of the hominoid humerus. Journal of Anatomy 221, 394-405.

Aubriot, J.H., 1981. The metacarpophalangeal joint of the thumb. The Hand 1, 184–187.

Barmakian, J.T., 1992. Anatomy of the joints of the thumb. Hand clinics 8, 683–691.

Bardo, A., Cornette, R., Borel, A., Pouydebat, E., 2017. Manual function and performance in humans, gorillas, and orangutans during the same tool use task. American Journal of Physical Anthropology 164, 821-836.

Bardo, A., Vigouroux, L., Kivell, T. L., Pouydebat, E., 2018. The impact of hand proportions on tool grip abilities in humans, great apes and fossil hominins: A biomechanical analysis using musculoskeletal simulation. Journal of human evolution 125, 106-121.

Berger, L.R., Ruiter, D.J. de, Churchill, S.E., Schmid, P., Carlson, K.J., Dirks, P.H.G.M., Kibii, J.M., 2010. *Australopithecus sediba*: A new species of *Homo*-like australopith from South Africa. Science 328, 195–204.

Berger, L.R., Hawks, J., Ruiter, D.J. de, Churchill, S.E., Schmid, P., Delezene, L.K., Kivell, T.L., Garvin, H.M., Williams, S.A., DeSilva, J.M., Skinner, M.M., Musiba, C.M., Cameron, N., Holliday, T.W., Harcourt-Smith, W., Ackermann, R.R., Bastir, M., Bogin, B., Bolter, D., Brophy, J., Cofran, Z.D., Congdon, K.A., Deane, A.S., Dembo, M., Drapeau, M., Elliott, M.C., Feuerriegel, E.M., Garcia-Martinez, D., Green, D.J., Gurtov, A., Irish, J.D., Kruger, A., Laird, M.F., Marchi, D., Meyer, M.R., Nalla, S., Negash, E.W., Orr, C.M., Radovcic, D., Schroeder, L., Scott, J.E., Throckmorton, Z., Tocheri, M.W., VanSickle, C., Walker, C.S., Wei, P., Zipfel, B., 2015. *Homo naledi*, a new species of the genus *Homo* from the Dinaledi Chamber, South Africa. eLife 4, e09560.

Boesch, C., Boesch, H., 1990. Tool use and tool making in wild chimpanzees. Folia Primatologica 54, 86–99.

Boesch, C., Boesch, H., 1993. Different hand postures for pounding nuts with natural hammers by wild chimpanzees. In: Preuschoft, P.D.H., Chivers, D.D.J. (Eds.), Hands of Primates. Springer, Wien, pp. 31–43.

Bojsen-Møller, F., 1976, Osteoligamentous guidance of the movements of the human thumb. American Journal of Anatomy 147, 71-79.

Bookstein, F.L., 1997. Landmark methods for forms without landmarks: morphometrics of group differences in outline shape. Medical Image Analysis 1, 225–243.

Bordes, F., 1961. Mousterian cultures in France: artifacts from recent excavation dispel some popular misconceptions about Neanderthal man. Science 134, 803–810.

Breuer, T., Ndoundou-Hockemba, M., Fishlock, V., 2005. First observation of tool use in wild gorillas. PLoS Biology 3, e380.

Bush, M.E., Lovejoy, C.O., Johanson, D.C., 1982. Hominid carpal, metacarpal, and phalangeal bones recovered from the Hadar formation: 1974–1977 collections. American Journal of Physical Anthropology 57, 651-677.

Byrne, R.W., Corp, N., Byrne, J.M., 2001. Manual dexterity in the gorilla: bimanual and digit role differentiation in a natural task. Animal Cognition 4, 347-361.

Carlson, K.J., Lublinsky, S., Judex, S., 2008. Do different locomotor modes during growth modulate trabecular architecture in the murine hind limb? Integrative and Comparative Biology 48, 385-393.

Christel, M., 1993. Grasping techniques and hand preferences in Hominoidea. In: Preuschoft, P.D.H., Chivers, D.D.J. (Eds.), Hands of Primates. Springer, Wien, pp. 91–108.

Churchill, S.E., 2001. Hand morphology, manipulation, and tool use in Neandertals and early modern humans of the Near East. Proceedings of the National Academy of Sciences USA 98, 2953-2955.

Clarke, R.J., 1999. Discovery of complete arm and hand of the 3.3 million-year-old A*ustralopithecus* skeleton from Sterkfontein. South African Journal of Science 95, 477–480.

Clarke, R.J., 2013. *Australopithecus* from Sterkfontein Caves, South Africa. In: Reed, K.E., Fleagle, J.G., Leakey R.E. (Eds), The Palaeobiology of *Australopithecus*. Springer, Dordrecht, pp. 105-123.

Conard, N.J., Richter, J. (Eds.), 2011. Neanderthal Lifeways, Subsistence and Technology: One Hundred Fifty Years of Neanderthal Study. Springer, New York.

Crast, J., Fragaszy, D., Hayashi, M., Matsuzawa, T., 2009. Dynamic in-hand movements in adult and young juvenile chimpanzees (*Pan troglodytes*). American Journal of Physical Anthropology 138, 274–285.

Crompton, R.H., Sellers, W.I., Thorpe, S.K.S., 2010. Arborelaity, terrestriality and bipedalism. Philosophical Transactions of the Royal Society B 365, 3301-3314.

De Groote, I., 2011. Femoral curvature in Neanderthals and modern humans: a 3D geometric analysis. Journal of Human Evolution 60, 540-548.

Diogo, R., Richmond, B.G., Wood, B., 2012. Evolution and homologies of primate and modern human hand and forearm muscles, with notes on thumb movements and tool use. Journal of Human Evolution 63, 64–78.

Dirks, P.H.G., Roberts, E.M., Hilbert-Wolf, H., Kramers, J.D., Hawks, J., Dosseto, A., Duval, M., Elliott, M.E.M., Grün, R., Hellstrom, J., Herries, A.I.R., Joannes-Boyau, R., Placzek, C.J., Robbins, J., Spandler, C., Wiersma, J., Woodhead, J., Berger, L.R., 2017. The age of *Homo naledi* and associated sediments in the rising star Cave, South Africa. eLife 6, e24231.

Domalain, M., Vigouroux, L., Danion, F., Sevrez, V., Berton, E., 2008. Effect of object width on precision grip force and finger posture. Ergonomics 51, 1441-1453.

Domínguez-Rodrigo, M., Pickering, T.R., Almécija S., Heaton, J.L., Baquedano, E., Mabulla, A., Uribelarrea, D. 2015. Earliest modern human-like hand bone from new >1.84-milion-year-old site at Olduvai in Tanzania. Nature Communications 6, 7987.

Doran, D.M., 1992. Comparison of instantaneous and locomotor bout sampling methods: a case study of adult male chimpanzee locomotor behavior and substrate use. American Journal of Physical Anthropology 89, 85-99.

Doran, D.M., 1996. Comparative positional behavior of the African apes. In: McGrew, W., Marchant, L.F., Nischida, T., (Eds.), Great Apes Societies. Cambridge University Press, Cambridge, pp. 213-224.

Doran, D.M., 1997. Ontogeny of locomotion in mountain gorillas and chimpanzees. Journal of Human Evolution 32, 323-344.

Douka, K., Spinapolice, E.E., 2012. Neanderthal shell tool production: evidence from middle palaeolithic Italy and Greece. Journal of World Prehistory 25, 45–79.

Drapeau, M.S., 2015. Metacarpal torsion in apes, humans, and early *Australopithecus*: implications for manipulatory abilities. PeerJ 3, e1311.

Dunn, R.H., Tocheri, M.W., Orr, C.M., Jungers, W.L., 2014. Ecological divergence and talar morphology in gorillas. American Journal of Physical Anthropology 153, 526-541.

Elliott, J.M., Connolly, K.J., 1984. A classification of manipulative hand movements. Developmental Medicine & Child Neurology 26, 283-296.

Fernández, P.J., Almécija, S., Patel, B.A., Orr, C.M., Tocheri, M.W., Jungers, W.L., 2015. Functional aspects of metatarsal head shape in humans, apes, and Old World monkeys. Journal of Human Evolution 86, 136–146.

Fernández, P.J., Mongle, C.S:, Leakey, L., Proctor, D.J., Orr, C.M., Patel, B.A., Almécija, S., Tocheri, M.W., Jungers, W.L, 2018. Evolution and function of the hominin forefoot. Proceedings of the National Academy of Sciences USA 115, 8746-8751.

Feuerriegel, E.M., Green, D.J., Walker, C.S., Schmid, P., Hawks, J., Berger, L.R., Churchill, S.E., 2017. The upper limb of *Homo naledi*. Journal of Human Evolution 104, 155–173.

Gower, J.C., 1975. Generalized Procrustes analysis. Psychometrika 40, 33–51.

Green, D.J., Gordon, A.D., 2008. Metacarpal proportions in *Australopithecus africanus*. Journal of Human Evolution 54, 705-719.

Grueter, C.C., Robbins, M.M., Ndagijimana, F., Stoinski, T.S., 2013. Possible tool use in a mountain gorilla. Behavioural Processes 100, 160–162.

Gunz, P., Mitteroecker, P., Bookstein, F.L., 2005. Semilandmarks in three dimensions. In: Slice, D.E. (Ed.), Modern Morphometrics in Physical Anthropology, Developments in Primatology: Progress and Prospects. Springer, Boston, pp. 73–98.

Haines, R.W., 1944. The mechanism of rotation at the first carpo-metacarpal joint. Journal of Anatomy 78, 44–46.

Hamrick, M.W., 1996. Articular size and curvature as determinants of carpal joint mobility and stability in strepsirrhine primates. Journal of Morphology 230, 113-127.

Hamrick, M.W., Inouye, S.E., 1995. Thumbs, tools, and early humans. Science 268, 586-587.

Hanna, J.B., Granatosky, M.C., Rana, P., Schmitt, D., 2017. The evolution of vertical climbing in primates: evidence from reaction forces. Journal of Experimental Biology 220, 3039-3052.

Harcourt-Smith, W.E., Aiello, L.C., 2004. Fossils, feet and the evolution of human bipedal locomotion. Journal of Anatomy 204, 403-416.

Harcourt-Smith, W.E., Throckmorton, Z., Congdon, K.A., Zipfel, B., Deane, A.S., Drapeau, M.S., Churchill, S.E., Berger, L.R., DeSilva, J.M., 2015. The foot of *Homo naledi*. Nature Communications 6, 8432.

Harmand, S., Lewis, J.E., Feibel, C.S., Lepre, C.J., Prat, S., Lenoble, A., Boës, X., Quinn, R.L., Brenet, M., Arroyo, A., Taylor, N., Clément, S., Daver, G., Brugal, J.-P., Leakey, L., Mortlock, R.A., Wright, J.D., Lokorodi, S., Kirwa, C., Kent, D.V., Roche, H., 2015. 3.3-million-year-old stone tools from Lomekwi 3, West Turkana, Kenya. Nature 521, 310–315.

Heim, J.-L., 1982. Les Hommes Fossiles de La Ferrassie. Tome II. Les Squelettes Adultes (Squelette des Membres). Masson, Paris.

Hirasaki, E., Kumakura, H., Matano, S., 1993. Kinesiological characteristics of vertical climbing in *Ateles geoffroyi* and *Macaca fuscata*. Folia Primatologica 61, 148-156.

Hunt, K.D., 1991. Positional behavior in the Hominoidea. International Journal of Primatology 12, 95-118.

Imaeda, T., An, K.-N., Cooney, W.P.I., 1992. Functional anatomy and biomechanics of the thumb. Hand Clinics 8, 9–15.

Jones-Engel, L.E., Bard, K.A., 1996. Precision grips in young chimpanzees. American Journal of Primatology 39, 1–15.

Jouffroy, F.K., Godinot, M., Nakano, Y., 1993. Biometrical characteristics of primate hands. In: Preuschoft, H., Chivers, D.J. (Eds.), Hands of Primates. Springer, Wien, pp. 133–171.

Judex, S., Garman, R., Squire, M., Donahue, L-R., Rubin, C., 2004. Genetically based influences on the site-specific regulation of trabecular and cortical bone morphology. Journal of Bone and Mineral Research 19, 600-606.

Karakostis, F.A., Hotz, G., Tourloukis, V., Harvati, K., 2018. Evidence for precision grasping in Neandertal daily activities. Science Advances 4, eaat2369.

Kivell, T.L., Kibii, J.M., Churchill, S.E., Schmid, P., Berger, L.R., 2011. *Australopithecus sediba* hand demonstrates mosaic evolution of locomotor and manipulative abilities. Science. 333, 1411–1417.

Kivell, T.L., Deane, A.S., Tocheri, M.W., Orr, C.M., Schmid, P., Hawks, J., Berger, L.R., Churchill, S.E., 2015. The hand of *Homo naledi*. Nature Communications 6, 8431.

Kivell, T.L., Lemelin, P., Richmond, B.G., Schmitt, D. (Eds.), 2016. The Evolution of the Primate Hand, Developments in Primatology: Progress and Prospects. Springer, New York.

Knigge, R.P., Tocheri, M.W., Orr, C.M., Mcnulty, K.P., 2015. Three-dimensional geometric morphometrics analysis of talar morphology in extant gorilla taxa from highland and lowland habitats. The Anatomical Record 298, 277-290.

Kuhn, S.L., 2014. Mousterian Lithic Technology: an Ecological Perspective. Princeton University Press, Princeton.

Kumar, S., Stecher, G., Suleski, M., Hedges, S. B., 2017. TimeTree: a resource for timelines, timetrees, and divergence times. Molecular Biology and Evolution 34, 1812–1819.

Lazenby, R.A., Angus, S., Cooper, D.M.L., Hallgrímsson, B., 2008. A three-dimensional microcomputed tomographic study of site-specific variation in trabecular microarchitecture in the human second metacarpal. Journal of Anatomy 213, 698–705.

Lewis, O.J., 1977. Joint remodelling and the evolution of the human hand. Journal of Anatomy 123, 157–201.

Li, Z.-M., Tang, J., 2007. Coordination of thumb joints during opposition. Journal of Biomechanics 40, 502–510.

Lieberman, D.E., Shea, J.J., 1994. Behavioral differences between archaic and modern humans in the Levantine Mousterian. American Anthropologist 96, 300–332.

Lockwood, C.A., Lynch, J.M., Kimbel, W.H., 2002. Quantifying temporal bone morphology of great apes and humans: an approach using geometric morphometrics. Journal of Anatomy 201, 447–464.

Lorenzo, C., Pablos, A., Carretero, J.M., Huguel, R., Valverdú, J., Martinón-Torres, M., Arsuaga, J.L., Carbonell, E., Bermúdez de Castro, J.M. 2015. Early Pleistocene human hand phalanx from the Sima del Elefante (TE) cave site in Sierra de Atapuerca (Spain). Journal of Human Evolution 78, 114-121.

Lovejoy, C.O., Heiple, K.G., Meindl, R.S., 2001. Palaeoanthropology: Did our ancestors knuckle-walk? Nature 410, 325-326.

Lovejoy, C.O., Simpson, S.W., White, T.D., Asfaw, B., Suwa, G., 2009. Careful climbing in the Miocene: the forelimbs of *Ardipithecus ramidus* and humans are primitive. Science 326, 70e1-70e8.

Marchi, D., 2005. The cross-sectional geometry of the hand and foot bones of the Hominoidea and

its relationship to locomotor behavior. Journal of Human Evolution 53, 743-761.

Marchi, D. Proctor, D.J., Huston, E., Nicholas, C.L., Fischer, F., 2017a. Morphological correlates of the first metacarpal proximal articular surface with manipulative capabilities in apes, humans and South African early hominins. Comptes Rendus Palevol 16, 645-654.

Marchi, D., Walker, C.S., Wei, P., Holliday, T.W., Churchill, S.E., Berger, L.R., DeSilva, J.M., 2017b. The thigh and leg of *Homo naledi*. Journal of Human Evolution 104, 174–204.

Marzke, M.W., 1983. Joint functions and grips of the *Australopithecus afarensis* hand, with special reference to the region of the capitate. Journal of Human Evolution 12, 197-211.

Marzke, M.W., 1997. Precision grips, hand morphology, and tools. American Journal of Physical Anthropology 102, 91–110.

Marzke, M.W., 2006. Who made stone tools? In: Roux, V., Bril, B. (Eds.), Stone Knapping: the Necessary Conditions for a Uniquely Hhominin Behaviour. McDonald Institute Monographs, Cambridge, pp. 243–255.

Marzke, M.W., 2013. Tool making, hand morphology and fossil hominins. Philosophical Transactions of the Royal Society B 368, 20120414.

Marzke, M.W., Marzke, R.F., 2000. Evolution of the human hand: approaches to acquiring, analysing and interpreting the anatomical evidence. Journal of Anatomy 197, 121–140.

Marzke, M.W., Shrewsbury, M.M., 2006. The *Oreopithecus* thumb: pitfalls in reconstructing muscle and ligament attachments from fossil bones Journal of Human Evolution 51, 213-215.

Marzke, M.W., Shackley, M.S., 1986. Hominid hand use in the pliocene and pleistocene: Evidence from experimental archaeology and comparative morphology. Journal of Human Evolution 15, 439–460.

Marzke, M.W., Wullstein, K.L., 1996. Chimpanzee and human grips: A new classification with a focus on evolutionary morphology. International Journal of Primatology 17, 117–139.

Marzke, M.W., Wullstein, K.L., Viegas, S.F., 1992. Evolution of the power ("squeeze") grip and its morphological correlates in hominids. American Journal of Physical Anthropology 89, 283-298.

Marzke, M.W., Tocheri, M.W., Steinberg, B., Femiani, J.D., Reece, S.P., Linscheid, R.L., Orr, C.M., Marzke, R.F., 2010. Comparative 3D quantitative analyses of trapeziometacarpal joint surface curvatures among living catarrhines and fossil hominins. American Journal of Physical Anthropology 141, 38–51.

Marzke, M.W., Marchant, L.F., McGrew, W.C., Reece, S.P., 2015. Grips and hand movements of chimpanzees during feeding in Mahale Mountains National Park, Tanzania. American Journal of Physical Anthropology 156, 317–326.

Matarazzo, S., 2013. Manual pressure distribution patterns of knuckle-walking apes. American Journal of Physical Anthropology 152, 44–50.

Matsuura, Y., Ogihara, N., Nakatsukasa, M., 2010. A method for quantifying articular surface morphology of metacarpals using quadric surface approximation. International Journal of Primatology 31, 263–274.

McHenry, H.M., 1986. The first bipeds: a comparison of the *A. afarensis* and *A. africanus* postcranium and implications for the evolution of bipedalism. Journal of Human Evolution 15, 177-191.

McPherron, S.P., Alemseged, Z., Marean, C.W., Wynn, J.G., Reed, D., Geraads, D., Bobe, R., Béarat, H.A., 2010. Evidence for stone-tool-assisted consumption of animal tissues before 3.39 million years ago at Dikika, Ethiopia. Nature 466, 857–860.

Midlo, C., 1934. Form of hand and foot in primates. American Journal of Physical Anthropology 19, 337–389.

Napier, J.R., 1955. The form and function of the carpo-metacarpal joint of the thumb. Journal of Anatomy 89, 362–369.

Napier, J.R., 1956. The prehensile movements of the human hand. The Journal of Bone and Joint Surgery 38B, 902–913.

Napier, J.R., 1960. Studies of the hands of living primates. Proceedings of the Zoological Society of London 134, 647–657.

Napier, J.R., 1993. Hands. Revised edition by Russell H. Tuttle. Princeton University Press, Princeton.

Neufuss, J., Robbins, M.M., Baeumer, J., Humle, T., Kivell, T.L., 2017. Comparison of hand use and forelimb posture during vertical climbing in mountain gorillas (*Gorilla beringei beringei*) and chimpanzees (*Pan troglodytes*). American Journal of Physical Anthropology 164, 651-664.

Neufuss, J., Robbins, M.M., Baeumer, J., Humle, T., Kivell, T.L., 2018. Manual skills for food processing by mountain gorillas (*Gorilla beringei beringei*) in Bwindi Impenetrable National Park, Uganda. Biological Journal of the Linnean Society. https://doi.org/10.1093/biolinnean/bly071

Niewoehner, W.A., 2000. The functional anatomy of late Pleistocene and recent human carpometacarpal and metacarpophalangeal articulations. Ph.D. Dissertation, University of New Mexico.

Niewoehner, W.A., 2005. A geometric morphometric analysis of late pleistocene human metacarpal 1 base shape. In: Slice, D.E. (Ed.), Modern Morphometrics in Physical Anthropology, Developments in Primatology: Progress and Prospects. Springer, Boston, pp. 285–298.

Niewoehner, W.A., 2006. Neanderthal hands in their proper perspective. In: Hublin, J.-J., Harvati, K., Harrison, T. (Eds.), Neanderthals Revisited: New Approaches and Perspectives. Springer, Dordrecht, pp. 157–190.

Niewoehner, W.A., Weaver, A.H., Trinkaus, E., 1997. Neandertal capitate-metacarpal articular morphology. American Journal of Physical Anthropology 103, 219–233.

Niewoehner, W.A., Bergstrom, A., Eichele, D., Zuroff, M., Clark, J.T., 2003. Digital analysis: manual dexterity in Neanderthals. Nature. 422, 395–395.

Parker, S.T., Kerr, M., Markowitz, H., Gould, J., 1999. A survey of tool use in zoo gorillas. In: Parker, S.T., Mitchell, R.W., Miles, H.L. (Eds.), The Mentalities of Gorillas and Orangutans. Cambridge University Press, Cambridge, pp. 188–193.

Patel, B.A., Maiolino, S.A., 2016. Morphological Diversity in the digital rays of primate hands. In: Kivell, T., Lemelin, P., Richmond, B.G., Schmitt, D., (Eds.), The Evolution of the Primate Hand. Springer, New York, pp. 55–100.

Pickering, R., Dirks, P.H.G.M., Jinnah, Z., de Ruiter, D.J., Churchill, S.E., Herries, A.I.R., Woodhead, J.D., Hellstrom, J.C., Berger, L.R., 2011. *Australopithecus sediba* at 1.977 Ma and implications for the origins of the genus *Homo*. *Science* 333,1421-1423.

Pouydebat, E., Gorce, P., Bels, V., 2009. Biomechanical study of grasping according to the volume of the object: human versus non-human primates. Journal of Biomechanics 42, 266-272.Pouydebat, E., Reghem, E., Borel, A., Gorce, P., 2011. Diversity of grip in adults and young humans and chimpanzees (*Pan troglodytes*). Behavioural Brain Research 218, 21–28.

Preuschoft, H., Chivers, D.J. (Eds.), 1993. Hands of Primates. Springer, Wien.

Proctor, D., 2010. Three-dimensional morphometrics of the proximal metatarsal articular surfaces of *Gorilla*, *Pan*, *Hylobates*, and shod and unshod humans. Ph.D. Dissertation, University of Iowa.

Proctor, D.J., Broadfield, D., Proctor, K., 2008. Quantitative three-dimensional shape analysis of the proximal hallucial metatarsal articular surface in *Homo*, *Pan*, *Gorilla*, and *Hylobates*. American Journal of Physical Anthropology 135, 216–224.

Pruetz, J. D., Tourkakis, C. A., Lindshield, S., 2009. Locomotion, posture and substrate use by west African chimpanzees (*Pan troglodytes verus*) in the savanna environment of Fongoli, Senegal. American Journal of Primatology 71, 90.

Rafferty, K.L., 1990. The functional and phylogenetic significance of the carpometacarpal joint of the thumb in anthropoid primates. M.S. Dissertation, New York University.

R Core Team, 2015. R: A language and environment for statistical computing. R Foundation for Statistical Computing, Wien.

Rein, T.R., Harrison, T., Carlson, K.J., Harvati, K., 2017. Adaptations to suspensory locomotion in *Australopithecus sediba*. Journal of Human Evolution 104, 1-12.

Remis, M., 1995. Effects of body size and social context on the arboreal activities of lowland gorillas in the Central African Republic. American Journal of Physical Anthropology 97, 413-433.

Remis, M., 1999. Tree structure and sex differences in arboreality among western lowland gorillas (*Gorilla gorilla gorilla*) at Bai Hokou, Central African Republic. Primates 40, 383-396.

Ricklan, D.E., 1987. Functional anatomy of the hand of *Australopithecus africanus*. Journal of Human Evolution 16, 643-664.

Ricklan, D.E., 1990. The precision grip in *Australopithecus africanus*: anatomical and behavioral correlates. In: Sperber, G.H. (Ed.), From Apes to Angels: Essays in Anthropology in Honor of Phillip V. Tobias. Wiley-Liss, New York, pp. 171–183.

Robinson, C., Terhune, C.E., 2017. Error in geometric morphometric data collection: Combining data from multiple sources. American Journal Physical Anthropology 164, 62-75.

Rohlf, F., 2010. tpsRelw: Relative warps analysis. Department of Ecology and Evolution, State University of New York at Stony Brook, Stony Brook, NY. http://life.bio.sunysb.edu/morph/morphmet/tpsrelww32.exe.

Rolian, C., Gordon, A.D., 2013. Reassessing manual proportions in *Australopithecus afarensis*. American Journal of Physical Anthropology 152, 393–406.

Rolian, C., Lieberman, D.E., Zermeno, J.P., 2011. Hand biomechanics during simulated stone tool use. Journal of Human Evolution 61, 26–41.

Rose, M.D., 1992. Kinematics of the trapezium-1st metacarpal joint in extant anthropoids and Miocene hominoids. Journal of Human Evolution 22, 255–266.

Ruff, C.B., 2003. Long bone articular and diaphyseal structure in Old World monkeys and apes. II: Estimation of body mass. American Journal of Physical Anthropology 120, 16-37.

Samuel, D.S., Nauwelaerts, S., Stevens, J.M.G., Kivell, T.L., 2018. Hand pressures during arboreal locomotion in captive bonobos (*Pan paniscus*). Journal of Experimental Biology 221, 1-18.

Schultz, A.H., 1930. The skeleton of the trunk and limbs of higher primates. Human Biology 2, 303-438.

Shea, J.J., 2003. The Middle Paleolithic of the east Mediterranean Levant. Journal of World Prehistory 17, 313–394.

Shearer, B.M., Cooke, S.B., Halenar, L.B., Reber, S.L., Plummer, J.E., Delson, E., Tallman, M., 2017. Evaluating causes of error in landmark-based data collection using scanners. PLoS One 12, e0187452.

Shigematsu, S., Shimizu, H., Beppu, M., Hirata, K., 2014. Anatomy of the extensor pollicis brevis associated with an extension mechanism of the thumb metacarpophalangeal joint. Hand Surgery 19, 171–179.

Shrewsbury, M.M., Marzke, M.W., Linscheis, R.L., Reece, S.P. 2003. Comparative morphology of the pollical distal phalanx. American Journal of Physical Anthropology 121, 30-47.

Skinner, M.M., Stephens, N.B., Tsegai, Z.J., Foote, A.C., Nguyen, N.H., Gross, T., Pahr, D.H., Hublin, J.-J., Kivell, T.L., 2015. Human-like hand use in *Australopithecus africanus*. Science 347, 395–399.

Stern, J.T. Jr., 2000. Climbing to the top: a personal memoir of *Australopithecus afarensis*. Evolutionary Anthropology 9, 113-133.

Stratford, D., Heaton, J.L., Pickering, T.R., Caruana, M.V., Shadrach, K. 2016. First hominin fossils from Milner Hall, Sterkfontein, South Africa. Journal of Human Evolution 91, 167-173.

Susman, R.L., 1979. Comparative and functional morphology of hominoid fingers. American Journal of Physical Anthropology 50, 215-236.

Susman, R.L., 1994. Fossil evidence for early hominid tool use. Science. 265, 1570–1573.

Susman, R.L., 1998. Hand function and tool behavior in early hominids. Journal of Human Evolution 35, 23–46.

Tafuri, M.A., Zangrando, A.F.J., Tessone, A., Kochi, S., Moggi-Cecchi, J., Di Vincenzo, J., Profico, A., Manzi, G., 2017. Dietary resilience among hunter-gatherers of Tierra del Fuego: isotopic evidence in a diachronic perspective. PLoS One 12, e0175594.

Thorpe, S.K.S., Crompton, R.H., 2006. Orangutan positional behavior and the nature of arboreal locomotion in Hominoidea. American Journal of Physical Anthropology 131, 384-401.

Tocheri, M.W., Marzke, M.W., Liu, D., Bae, M., Jones, G.P., Williams, R.C., Razdan, A., 2003. Functional capabilities of modern and fossil hominid hands: three-dimensional analysis of trapezia. American Journal of Physical Anthropology 122, 101–112.

Tocheri, M.W., Razdan, A., Williams, R.C., Marzke, M.W., 2005. A 3D quantitative comparison of trapezium and trapezoid relative articular and nonarticular surface areas in modern humans and great apes. Journal of Human Evolution 49, 570–586.

Tocheri, M.W., Orr, C.M., Jacofsky, M.C., Marzke, M.W., 2008. The evolutionary history of the hominin hand since the last common ancestor of *Pan* and *Homo*. Journal of Anatomy 212, 544–562.

Torigoe, T., 1985. Comparison of object manipulation among 74 species of non-human primates. Primates 26, 182–194.

Treece, G., Prager, R., Gee, A., 2013. The Stradwin 3D ultrasound acquisition and visualization system. Medical Imaging Group, Cambridge University Engineering Department, Cambridge. http://mi.eng.cam.ac.uk/~rwp/stradwin/.

Trinkaus, E., 1983. The Shanidar Neandertals. Academic Press, New York.

Trinkaus, E., 1985. Pathology and the posture of the La Chaleppe-aux-Saints Neandertal. American Journal of Physical Anthropology 67, 19-41.

Trinkaus, E., 1989. Olduvai hominid 7 trapezial metacarpal 1 articular morphology: Contrasts with recent humans. American Journal of Physical Anthropology 80, 411–416.

Trinkaus, E., Villemeur, I., 1991. Mechanical advantages of the Neandertal thumb in flexion: A test of an hypothesis. American Journal of Physical Anthropology 84, 249–260.

Turq, A., Roebroeks, W., Bourguignon, L., Faivre, J.-P., 2013. The fragmented character of Middle Palaeolithic stone tool technology. Journal of Human Evolution 65, 641–655.

Tuttle, R.H., 1967. Knuckle-walking and the evolution of hominoid hands. American Journal of Physical Anthropology 26, 171–206.

Tuttle, R.H., 1969. Quantitative and functional studies on the hands of the Anthropoidea. I. The Hominoidea. Journal of Morphology 128, 309–363.

Tuttle, R.H., 1981. Evolution of hominid bipedalism and prehensile capabilities. Philosophical Transaction of the Royal Society B 292, 89–94.

Tuttle, R.H., Rogers, C., 1966. Genetic and selective factors in reduction of the hallux in *Pongo pygmaeus*. American Journal of Physical Anthropology 24, 191-198.

Ward, C.V., 2002. Interpreting the posture and locomotion of *Australopithecus afarensis*: where do we stand? American Journal of Physical Anthropology 119, 185-215.

Ward, C.V., Kimbel, W.H., Harmon, E.H., Johanson, D.C:, 2012. New postcranial fossils of *Australopithecus afarensis* from Hadar, Ethiopia (1990-2007). Journal of Human Evolution 63, 1-51.

Ward, C.V., Tocheri, M.W., Plavcan, J.M., Brown, F.H., Manthi, F.K., 2014. Early Pleistocene third metacarpal from Kenya and the evolution of modern human-like hand morphology. Proceedings of the National Academy of Sciences USA 111, 121-124.

Wiley, D.F., Amenta, N., Alcantara, D., Ghosh, D., Kil, Y.J., Delson, E., Harcourt-Smith, W., Rohlf, F.J., St John, K., Hamann, B., 2005. Evolutionary morphing. In: Proceedings of the IEEE Visualization Conference 2005, IEEE, pp. 431–438.

Williams, S.A., García-Martínez, D., Bastir, M., Meyer, M.R., Nalla, S., Hawks, J., Schmid, P., Churchill, S.E., Berger, L.R., 2017. The vertebrae and ribs of *Homo naledi*. Journal of Human Evolution 104, 136–154.

Wunderlich, R.E., Jungers, W.L., 2009. Manual digital pressures during knuckle-walking in chimpanzees (*Pan troglodytes*). American Journal of Physical Anthropology 139, 394–403.

Young, R.W., 2003. Evolution of the human hand: the role of throwing and clubbing. Journal of Anatomy 202, 165–174.

764

Figures captions

Figure 1. Landmark setting. a) 5×5 patch placement on the distal articular surface of the first metacarpal. Fixed landmarks are represented by black, numbered dots and surface semilandmarks are represented by smaller gray dots at the nodes of the grid. From left to right: palmarulnar view, distal view, dorsoradial view. Definition of numbered landmarks is in Table 2. b) Morphological characteristics highlighted by the landmark setting.

Figure 2. Three-dimensional rendering of a typical left metacarpal 1 head morphology for each of the extant species and of three fossil hominin specimens studied here. *Homo sapiens*, State Anthropological Collection, Munich, specimen number 186; *Pan troglodytes*, State Zoological Collection, Munich, specimen number 1955-25; *Gorilla gorilla*, Shultz Collection, University of Zurich Irchel, specimen number 8; *Pongo pygmaeus*, State Zoological Collection, Munich, specimen number 1909-801; *Homo naledi*, specimen number U.W. 101-1282; *Homo neanderthalensis*, specimen number Tabun C1; *Australopithecus africanus*, specimen number StW 418.

Figure 3. Scatterplot of the second vs. the first principal component (PC2 vs. PC1) scores of extant samples (*Homo* labeled *'Humans'* in figure, *Pan*, *Gorilla*, and *Pongo*) and fossil specimens Tabun C1 and La Chapelle-aux-Saints (*Homo neanderthalensis* labeled 'Neanderthal' in figure), U.W. 101-1282 (*Homo naledi*), U.W. 88-119 (*Australopithecus sediba*), SK 84 (*Paranthropus robustus*/early *Homo*), StW 418 (*Australopithecus africanus*) and A.L. 333w-39 (*Australopithecus afarensis*). The mesh/wireframes show extreme shape for each axis. For each mesh/wireframe, radial is on the left, dorsal is superiorly. Meshes/wireframes are shown from three different points of view, from top to bottom or from left to right: distal view, radial view, palmar view.

Figure 4. Scatterplot of the third vs. the first principal component (PC3 vs. PC1) scores of extant samples (*Homo* labeled *'Humans'* in figure, *Pan*, *Gorilla*, and *Pongo*) and fossil specimens Tabun C1 and La Chapelle-aux-Saints (*Homo neanderthalensis* labeled 'Neanderthal' in figure), U.W. 101-1282 (*Homo naledi*), U.W. 88-119 (*Australopithecus sediba*), SK 84 (*Paranthropus*

robustus/early *Homo*), StW 418 (*Australopithecus africanus*) and A.L. 333w-39 (*Australopithecus afarensis*). The mesh/wireframes show extreme shape for each axis. For each mesh/wireframe, radial is on the left, dorsal is superiorly. Meshes/wireframes are shown from three different points of view, from top to bottom or from left to right: distal view, radial view, palmar view.

Figure 5. Boxplot of the first principal component (PC1) scores for *Homo sapiens* (labeled 'Humans' in figure), *Pan*, *Gorilla* and *Pongo* compared to fossil specimens Tabun C1 and La Chapelle-aux-Saints (*Homo neanderthalensis* labeled 'Neanderthal' in figure), U.W. 101-1282 (*Homo naledi*), U.W. 88-119 (*Australopithecus sediba*), SK 84 (*Paranthropus robustus*/early *Homo*), StW 418 (*Australopithecus africanus*) and A.L. 333w-39 (*Australopithecus afarensis*). Black lines are the medians, boxes are the interquartile ranges, whiskers are the non-outlier ranges and empty circles are outliers.

Figure 6. Boxplot of the second principal component (PC2) scores for *Homo sapiens* (labeled 'Humans' in figure), *Pan*, *Gorilla* and *Pongo* compared to fossil specimens Tabun C1 and La Chapelle-aux-Saints (*Homo neanderthalensis* labeled 'Neanderthal' in figure), U.W. 101-1282 (*Homo naledi*), U.W. 88-119 (*Australopithecus sediba*), SK 84 (*Paranthropus robustus*/early *Homo*), StW 418 (*Australopithecus africanus*) and A.L. 333w-39 (*Australopithecus afarensis*). Black lines are the medians, boxes are the interquartile ranges, whiskers are the non-outlier ranges and empty circles are outliers.

Figure 7. Boxplot of the third principal component (PC3) scores for *Homo sapiens* (labeled 'Humans' in figure), *Pan*, *Gorilla* and *Pongo* compared to fossil specimens Tabun C1 and La Chapelle-aux-Saints (*Homo neanderthalensis* labeled 'Neanderthal' in figure), U.W. 101-1282 (*Homo naledi*), U.W. 88-119 (*Australopithecus sediba*), SK 84 (*Paranthropus robustus*/early *Homo*), StW 418 (*Australopithecus africanus*) and A.L. 333w-39 (*Australopithecus afarensis*). Black lines are the medians, boxes are the interquartile ranges, whiskers are the non-outlier ranges and empty circles are outliers.

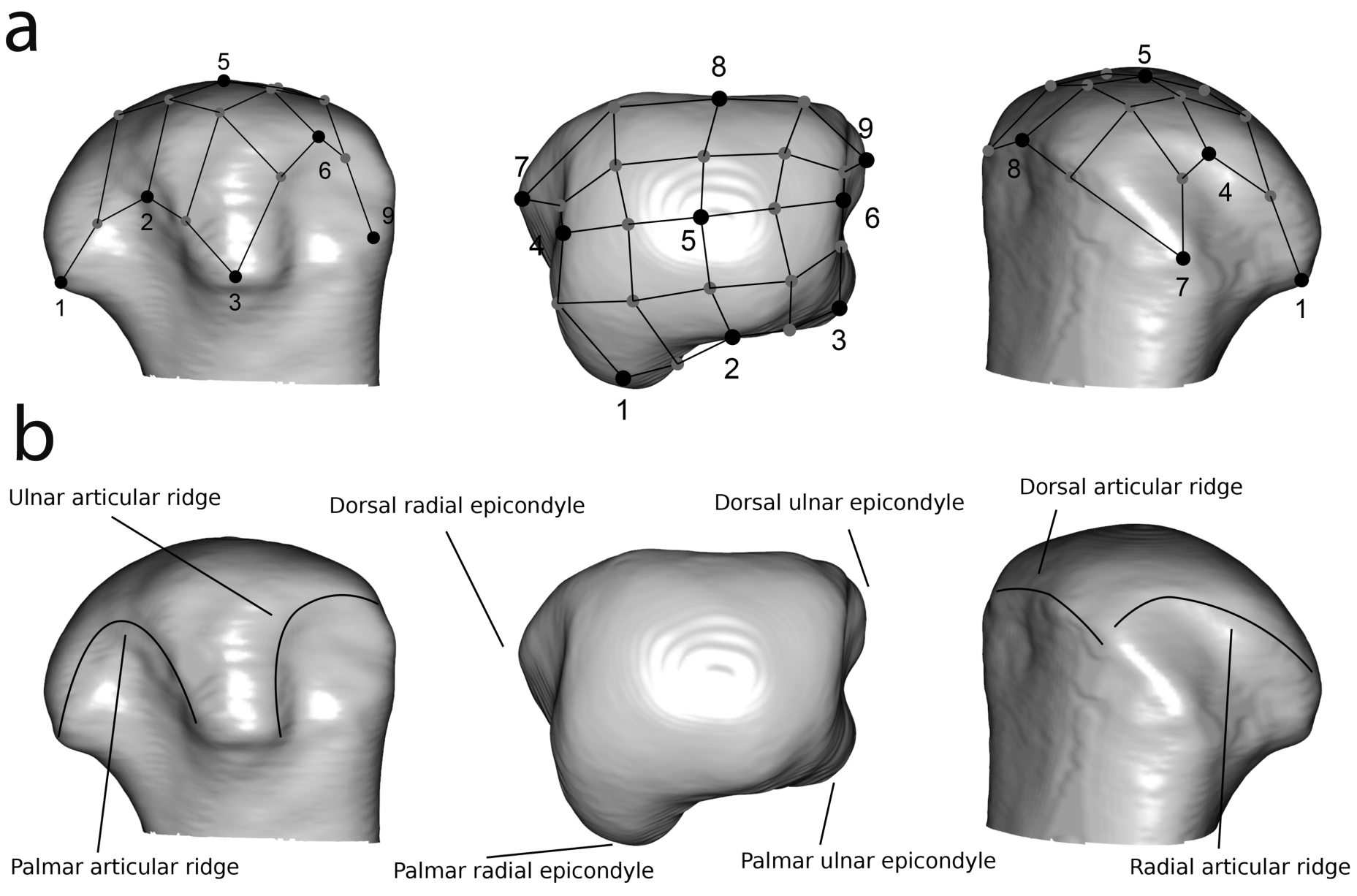
a
5
6
2
9
1
3
8
9
7
6
4
5
3
2
1
5
8
4
7
1
b
Ulnar articular ridge
Dorsal radial epicondyle
Dorsal ulnar epicondyle
Dorsal articular ridge
Palmar articular ridge
Palmar radial epicondyle
Palmar ulnar epicondyle
Radial articular ridge

Homo sapiens

Pan troglodytes

Pongo pygmaeus

Gorilla gorilla

U.W. 101-1282

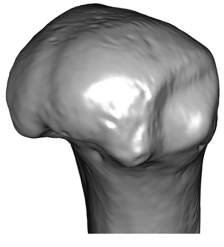

Tabun C1

StW 418

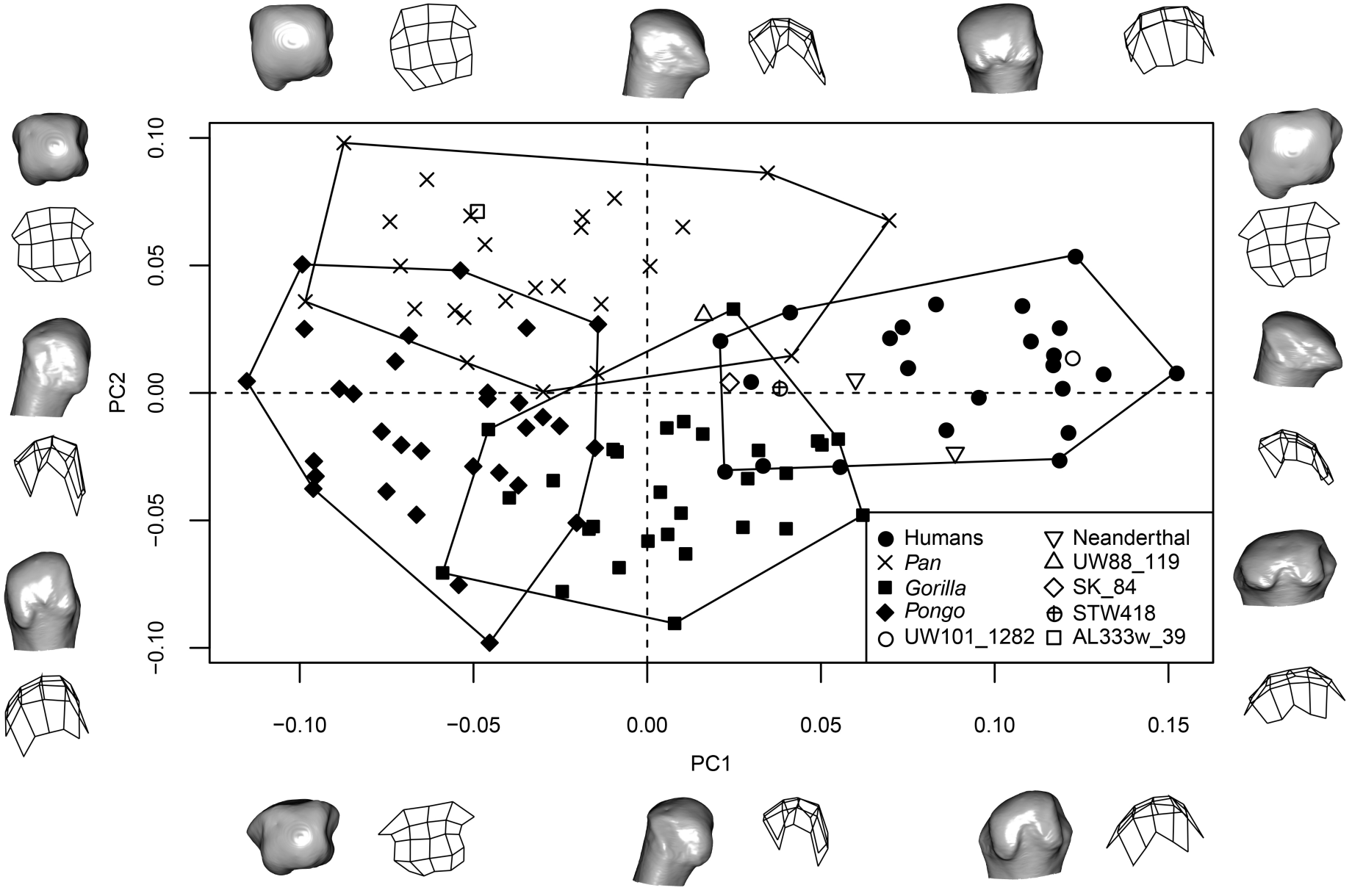
PC2
0.10
0.05
0.00
−0.05
−0.10
−0.10
−0.05
0.00
0.05
0.10
0.15
PC1
Humans
Pan
Gorilla
Pongo
UW101_1282
Neanderthal
UW88_119
SK_84
STW418
AL333w_39

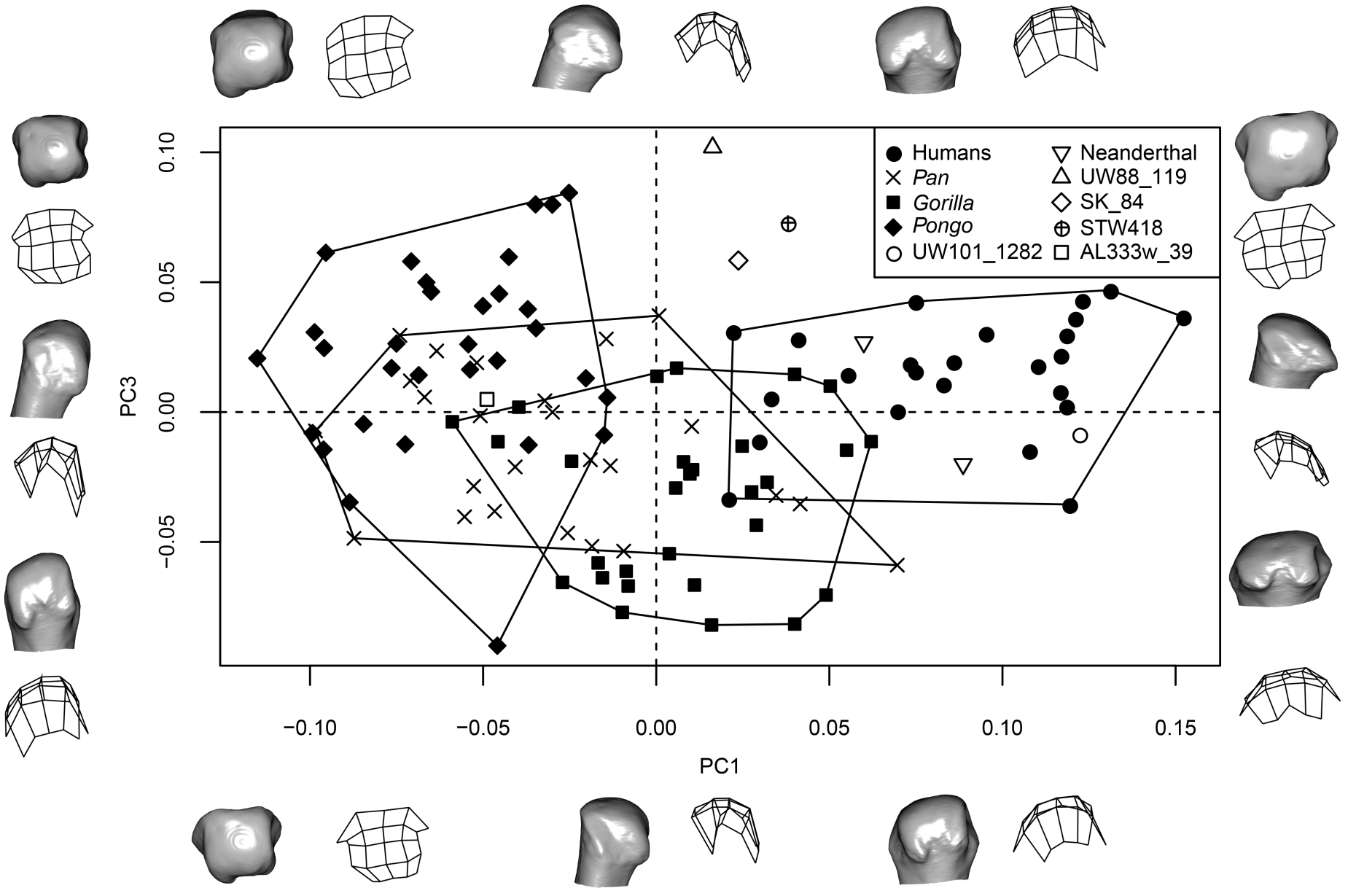
Humans
Pan
Gorilla
Pongo
UW101_1282
Neanderthal
UW88_119
SK_84
STW418
AL333w_39
PC3
PC1
0.10
0.05
0.00
−0.05
−0.10
−0.05
0.00
0.05
0.10
0.15

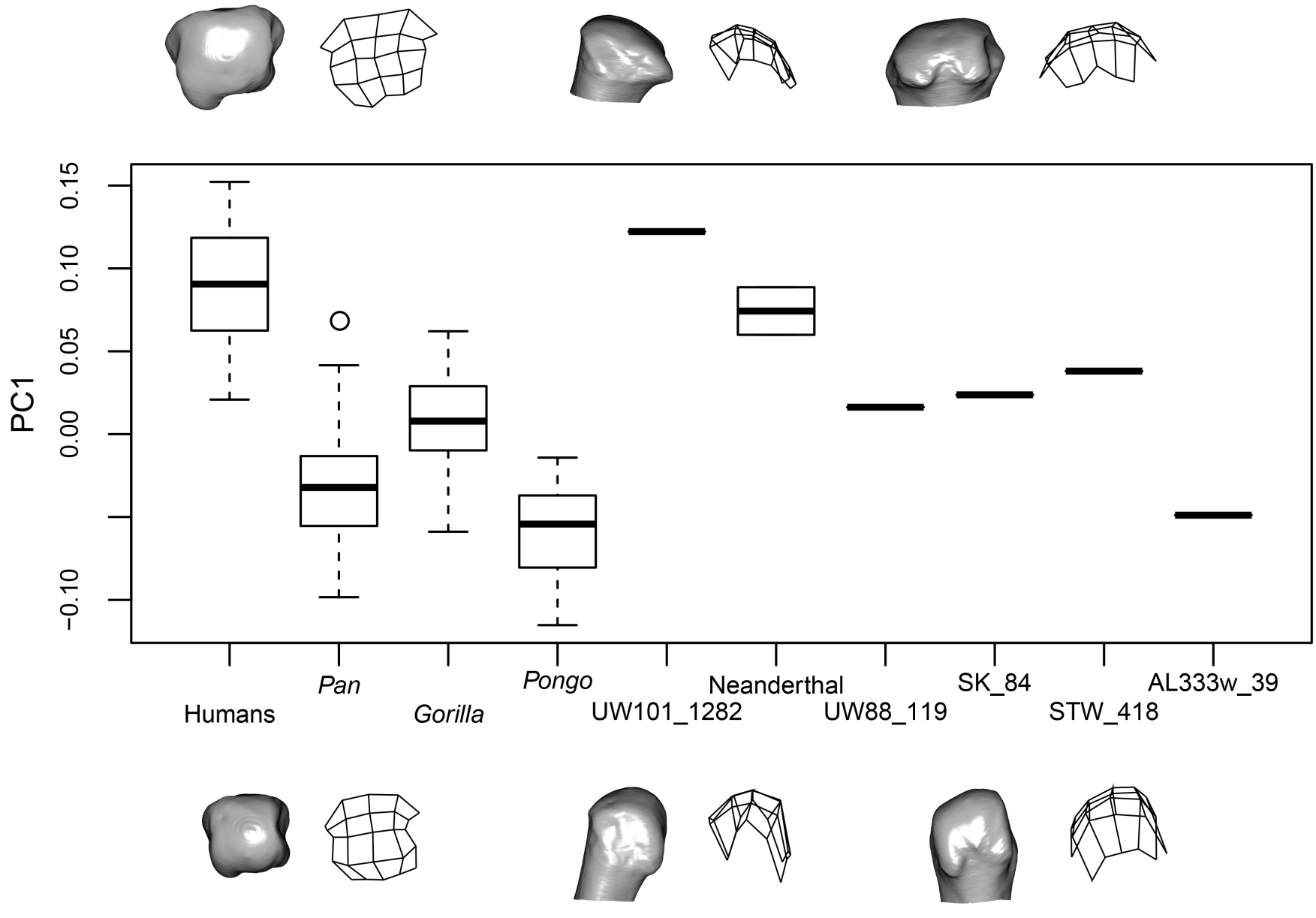
PC1
0.15
0.10
0.05
0.00
−0.10
Humans
Pan
Gorilla
Pongo
UW101_1282
Neanderthal
UW88_119
SK_84
STW_418
AL333w_39

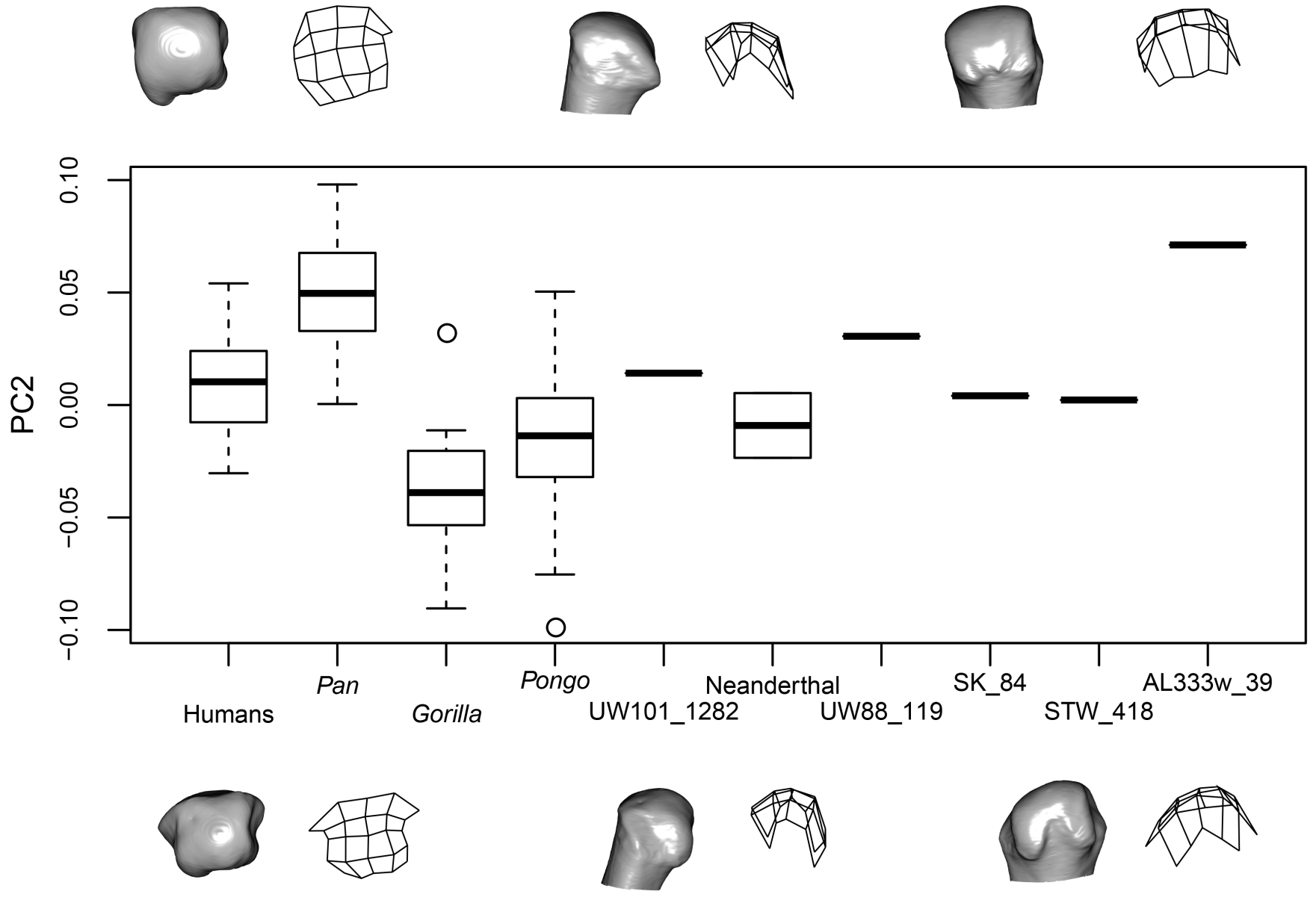
PC2
0.10
0.05
0.00
−0.05
−0.10
Humans
Pan
Gorilla
Pongo
UW101_1282
Neanderthal
UW88_119
SK_84
STW_418
AL333w_39

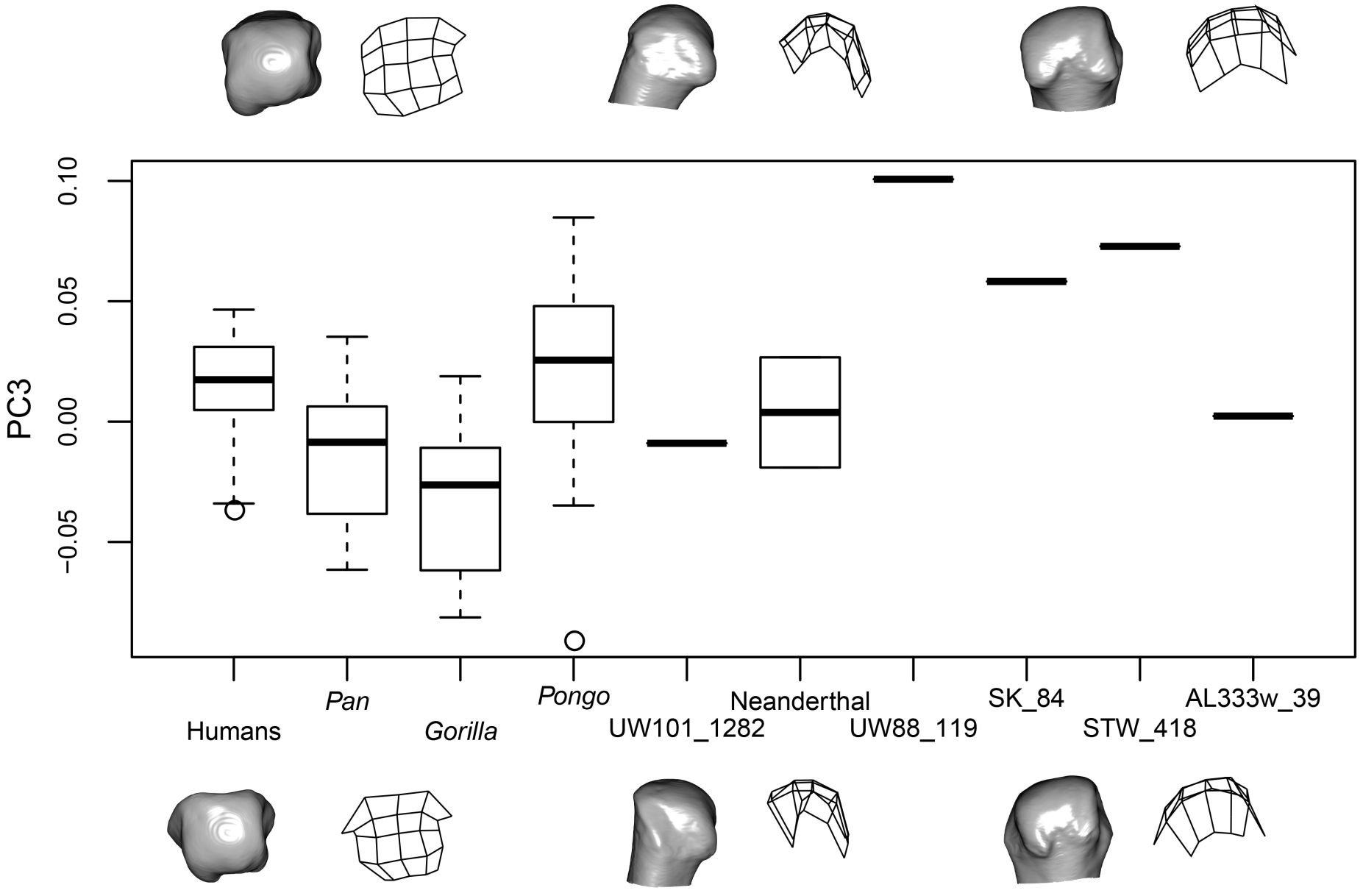
PC3
0.10
0.05
0.00
−0.05
Humans
Pan
Gorilla
Pongo
UW101_1282
Neanderthal
UW88_119
SK_84
STW_418
AL333w_39

Supplementary Online Material (SOM):

Three-dimensional geometric morphometric analysis of the first metacarpal distal articular surface in humans, great apes and fossil hominins

Lorenzo Galletta[a], Nicholas B. Stephens[b], Ameline Bardo[c], Tracy L. Kivell[c,d,e], Damiano Marchi[f,e*]

[a] *Centre for Integrative Ecology, Deakin University, 75 Pigdons Road, Waurn Ponds, 3216, VIC, Australia*

[b] *Department of Anthropology, The Pennsylvania State University, University Park, PA 1680, USA*

[c] *Animal Postcranial Evolution Lab, Skeletal Biology Research Centre, School of Anthropology and Conservation, University of Kent, Canterbury, CT2 7NR, UK*

[d] *Department of Human Evolution, Max Planck Institute for Evolutionary Anthropology, Deutscher Platz 6, Leipzig, 04103, Germany*

[e] *Evolutionary Studies Institute and Centre for Excellence in PalaeoSciences, University of the Witwatersrand, Private Bag 3, Wits 2050, South Africa*

[f] *Department of Biology, University of Pisa, Via Derna 1, Pisa, 56126, Italy*

* Corresponding author.

E-mail address: damiano.marchi@unipi.it (D. Marchi).

SOM S1

Procedure followed to correct the slight erosion on *Homo naledi* left first metacarpal (MC1) (U.W. 101-1282).

The U.W. 101-1282 *H. naledi* MC1 has slight erosion on the palmar-ulnar side of the distal epiphysis (Fig. 1). A smooth triangulated mesh was generated in Strandwin 5.2 (Treece et al., 2013) to estimate the original surface of the entire MC1, which was guided by contours placed every 10 tomographic slices along the z-axis. In order to preserve surface features for landmarking, a high-resolution mesh was generated with a polygon for each voxel in the tomographic scan. Following this, Geomagic Wrap (3D Systems) was used to extract the surface from the high-resolution mesh, which was then registered to the smooth mesh and merged (Fig. 2).

SOM S2

Principal component 4 analysis

A bivariate scatterplot of PC1 against PC4 (SOM Fig. S9) mainly divides *Pongo* and modern humans with the former occupying mainly the two left quadrants of the scatterplot and the latter the two left quadrants. However, a clear pattern of division among genera is not present and the four groups overlap extensively. La Chapelle-aux-Saints, StW 418 and SK 84 fall within the modern humans morphospace and Tabun C1 just outside it but very close. Both U.W. 88-119 and A.L. 333w-39 fall in the African apes, with the former closer to the human distribution and the latter far away and in the *Pongo*/*Pan* morphospace.

PC4 shape and groupings

The shape modifications described by PC4 do not distinguish much among groups (SOM Fig. S10; SOM Table S4). The negative side of the PC4 axis is occupied primarily by *Pan* and describes a shape with an articular surface that is radioulnarly flatter, a quadrate contour of the articular surface, and relatively small epicondyles. The positive aspect of PC4 axis, occupied mostly by *Gorilla* is characterized by larger epicondyles, a radial palmar condyle projecting more radially, and a more curved articular surface in the radioulnar plane. All fossils, with the exclusion of U.W. 101-1282 and Neanderthals, fall in the human and *Pongo* interquartile range, but high overlap with the African apes is present. *Homo naledi* (U.W. 101-1282) falls in the lower quartile of all extant groups and more than 1SD away from humans. Neanderthals fall in the upper quartile range of humans, *Gorilla* and *Pongo* with La Chapelle-aux-Saints not significantly different from human (within 1 SD of humans mean) and Tabun C1 more than 1 SD higher than humans and great apes (Fig. S10; SOM Table S4).

SOM Figure S1. Palmar view of voxel to vertex mesh created in Avizo 8.1 of first metacarpal of *Homo naledi* (U.W. 101-1282).

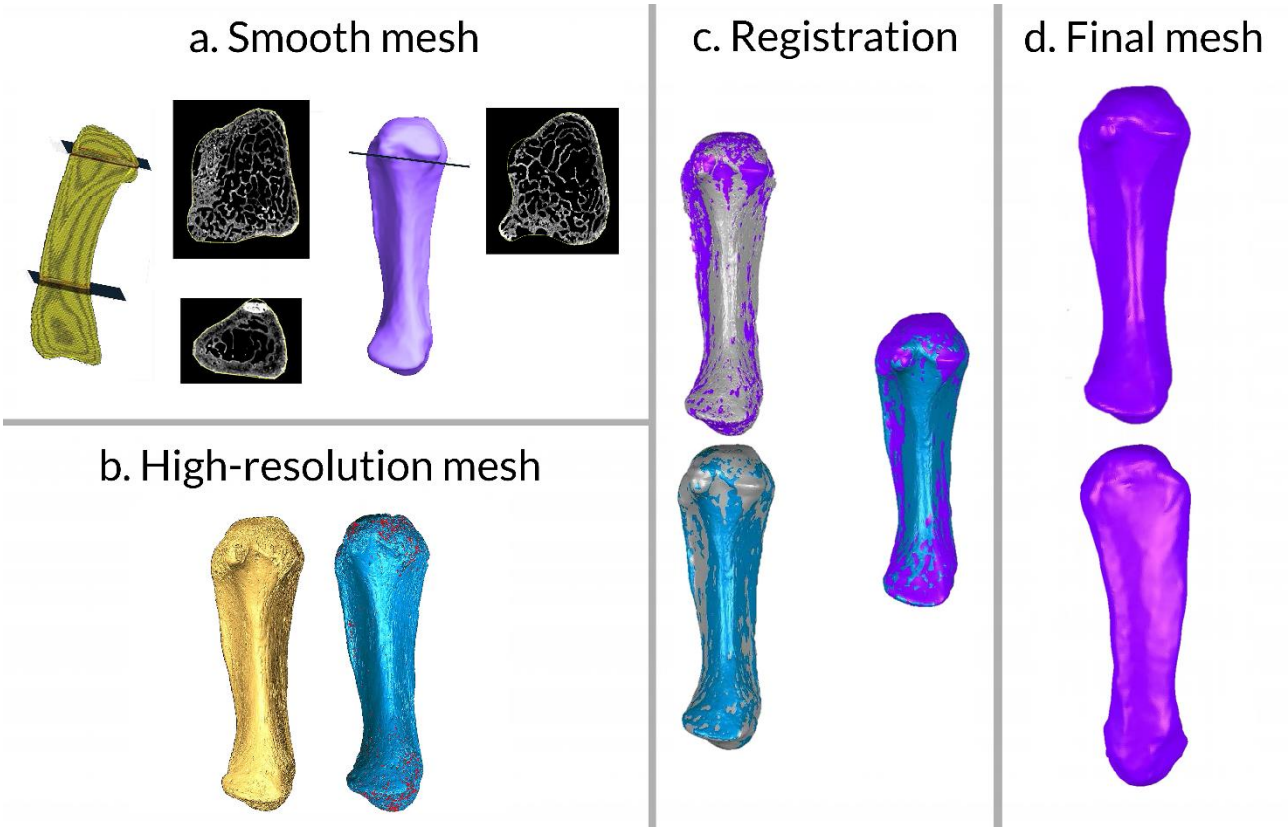

SOM Figure S2. a) Sample of the tomographic slices and guiding contours used to generate the smooth mesh from the U.W. 101-1282 MC1. b) Voxel based high-resolution mesh and extracted surface. c) Registration of high-resolution mesh in blue and smooth-mesh in purple. Note the grey area indicates the difference between the two surfaces prior to registration. d) The result of the two registered surfaces following merging in palmar and dorsal view.

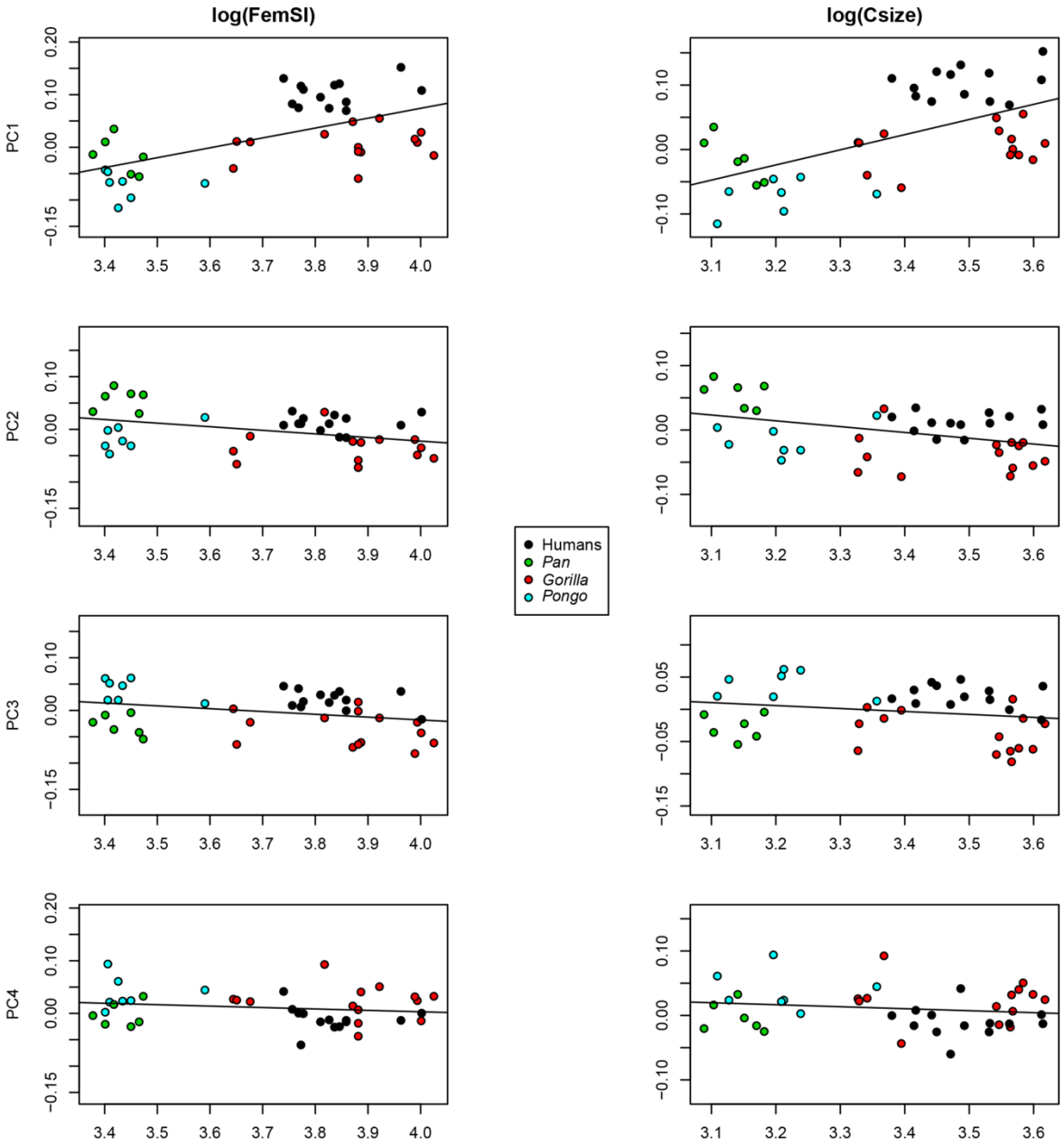

SOM Figure S3. Comparison of linear regression of scores of PC1–PC4 on natural log-transformed femoral superoinferior diameter (log(FemSI)) and natural log-transformed (centroid size) (log(Csize)).

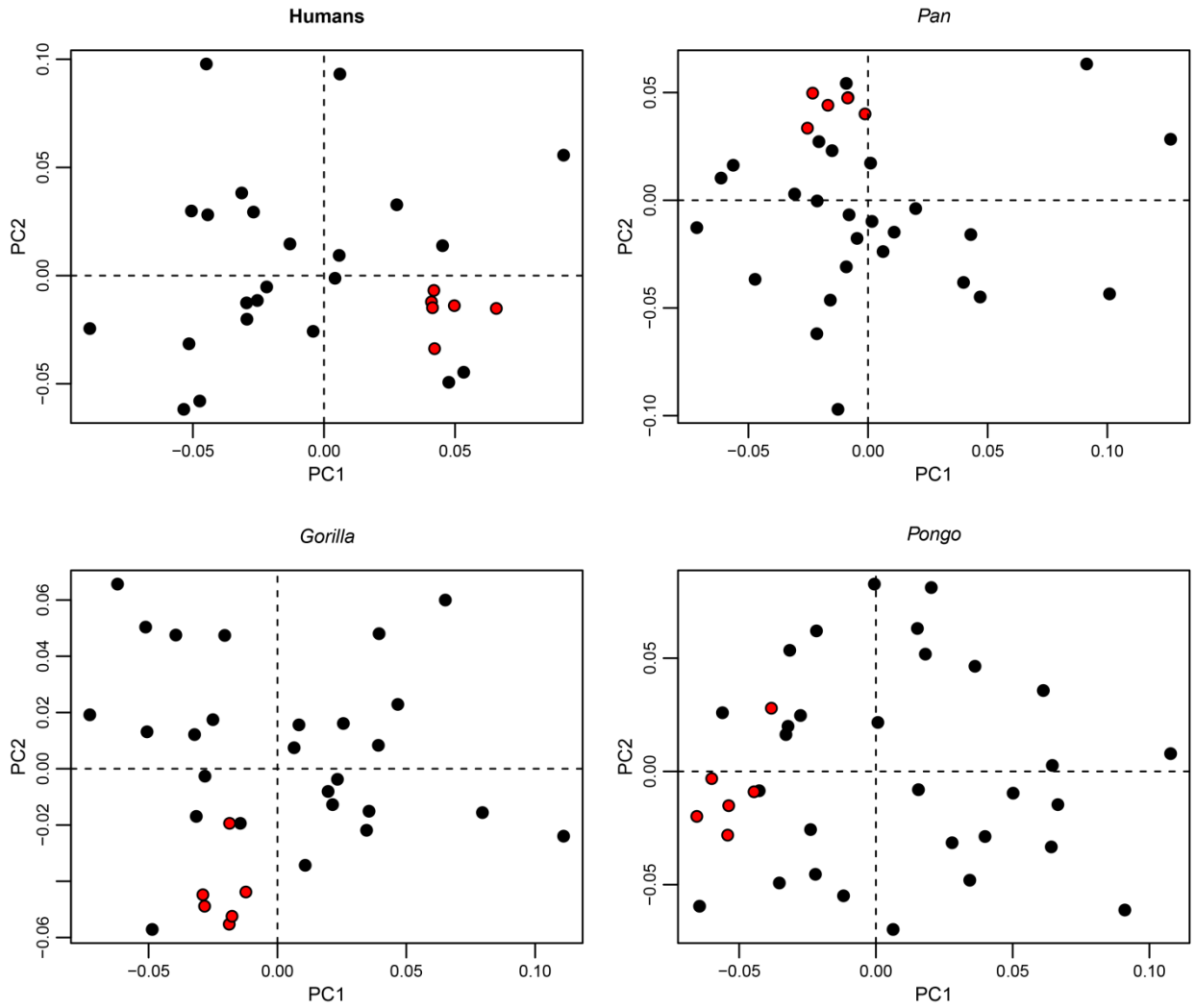

SOM Figure S4. Scatterplot of PC2 against PC1 as resulted from repeatability tests. Black circles are single individuals, red circles are repeated measures.

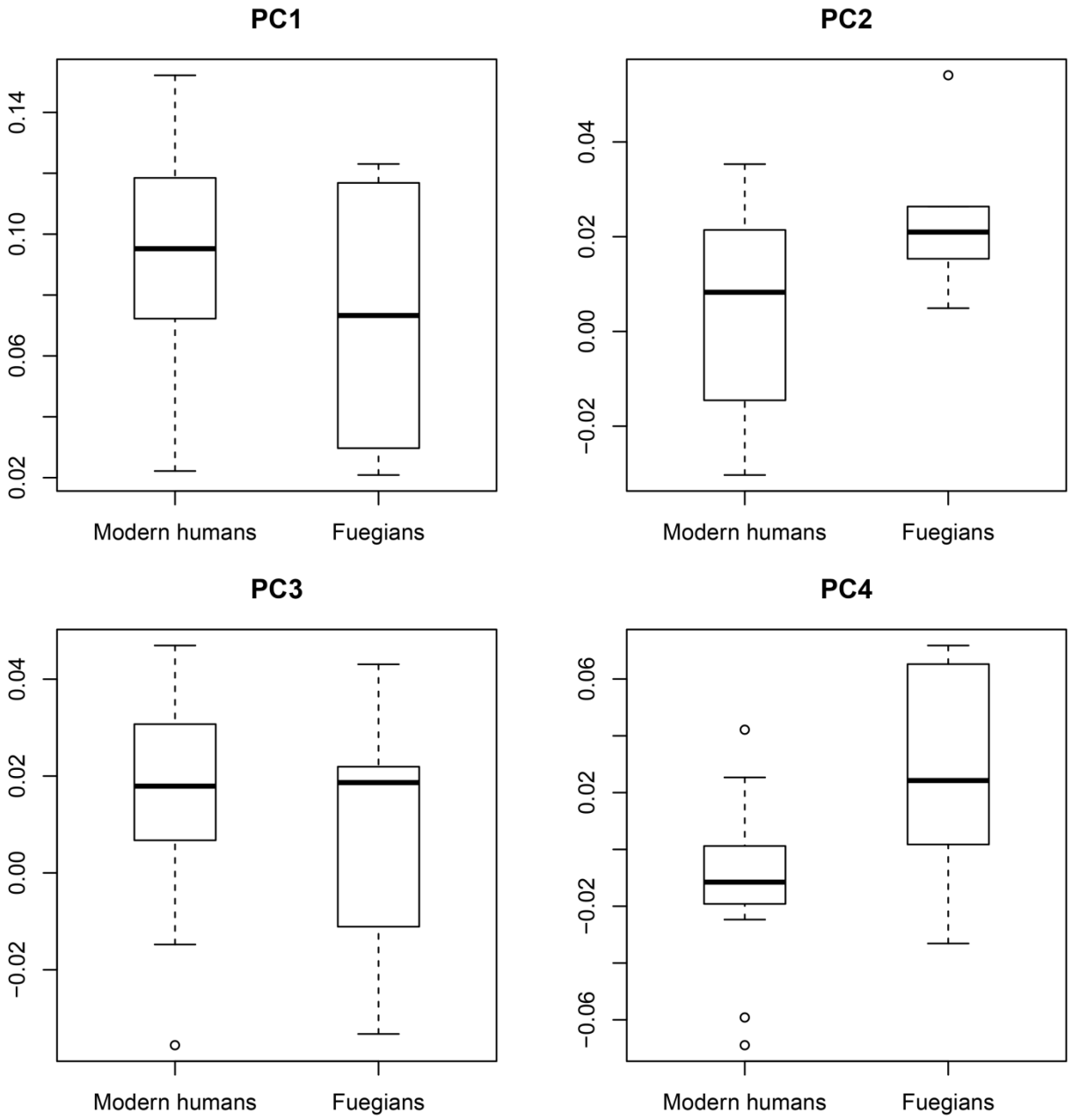

SOM Figure S5. Boxplot of the comparison between PC1–PC4 of Fuegians (hunter-gatherers) and the rest of the modern human sample.

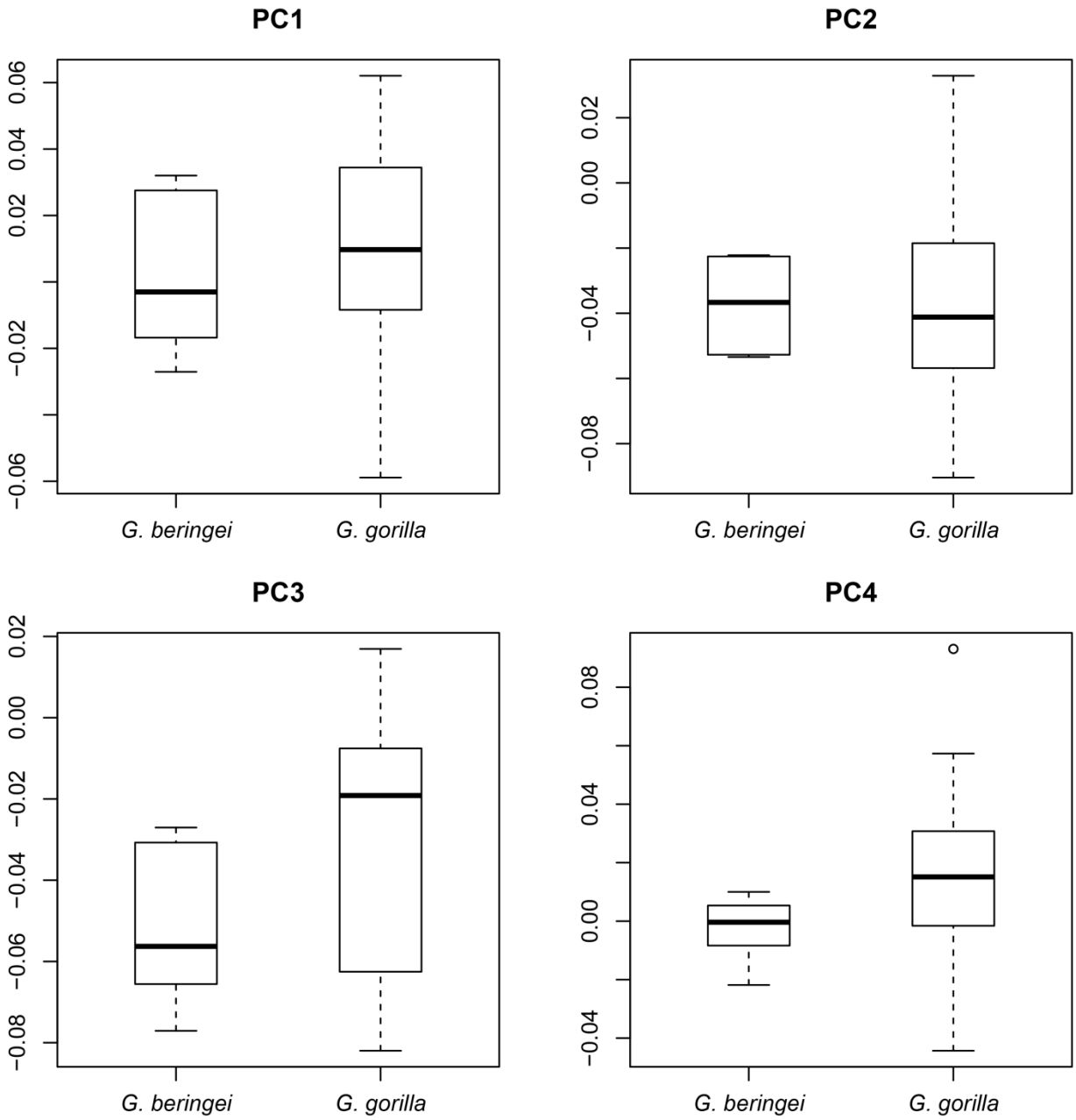

SOM Figure S6. Boxplot of the comparison between PC1–PC4 of *Gorilla beringei* and *Gorilla gorilla*.

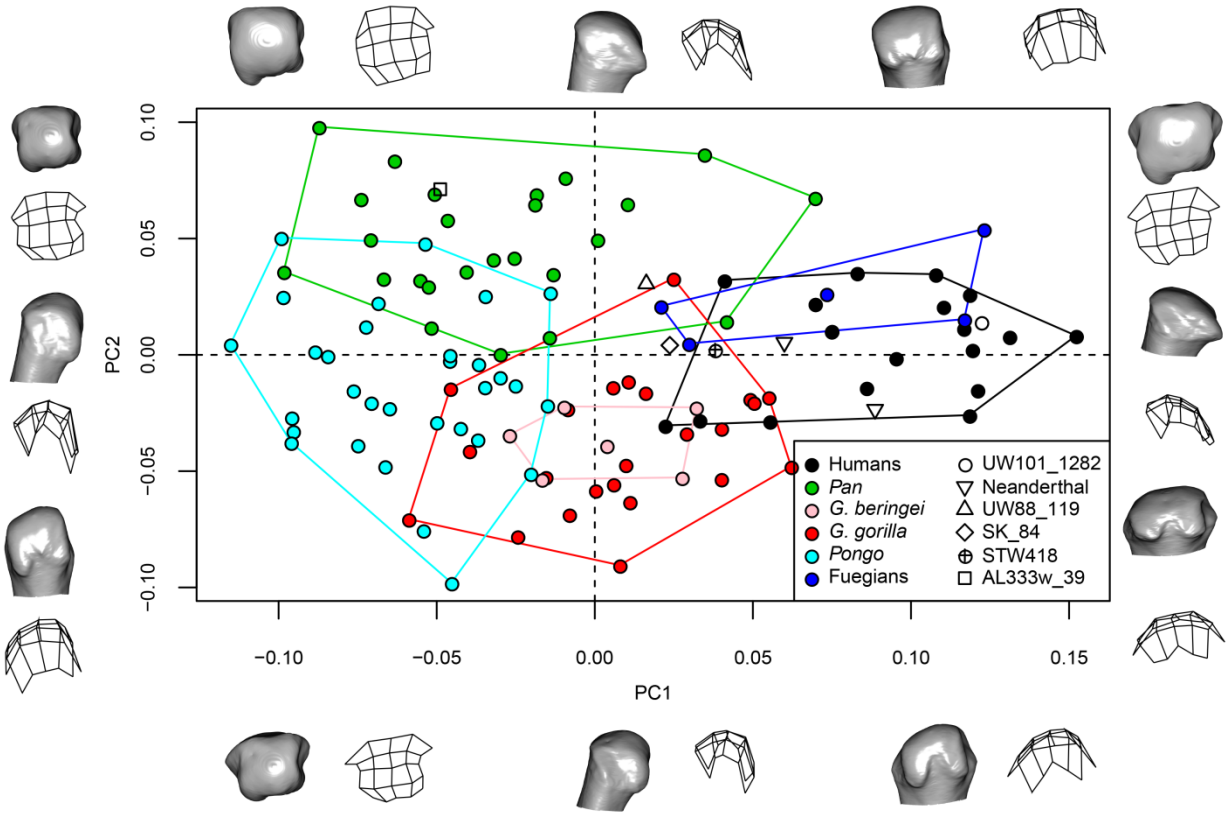

SOM Figure S7. Scatterplot of the second vs. the first principal component (PC2 vs. PC2) scores of extant samples (non-Fuegian *Homo sapiens* labeled 'Humans' in figure, *H. sapiens* from Tierra del Fuego labeled 'Fuegians' in figure, *Pan*, *Gorilla gorilla*, *Gorilla beringei* and *Pongo*) and fossil specimens Tabun C1 and La Chapelle-aux-Saints (*Homo neanderthalensis* labelled Neanderthal in figure), U.W. 101-1282 (*Homo naledi*), U.W. 88-119 (*Australopithecus sediba*), SK 84 (*Paranthropus robustus*/*Homo erectus*), StW 418 (*Australopithecus africanus*) and A.L. 333w-39 (*Australopithecus afarensis*). The mesh/wireframes show extreme shape for each axis. For each mesh/wireframe, radial is on the left, dorsal is superiorly. Meshes/wireframes are shown from three different points of view, from top to bottom or from left to right: distal view, radial view, palmar view.

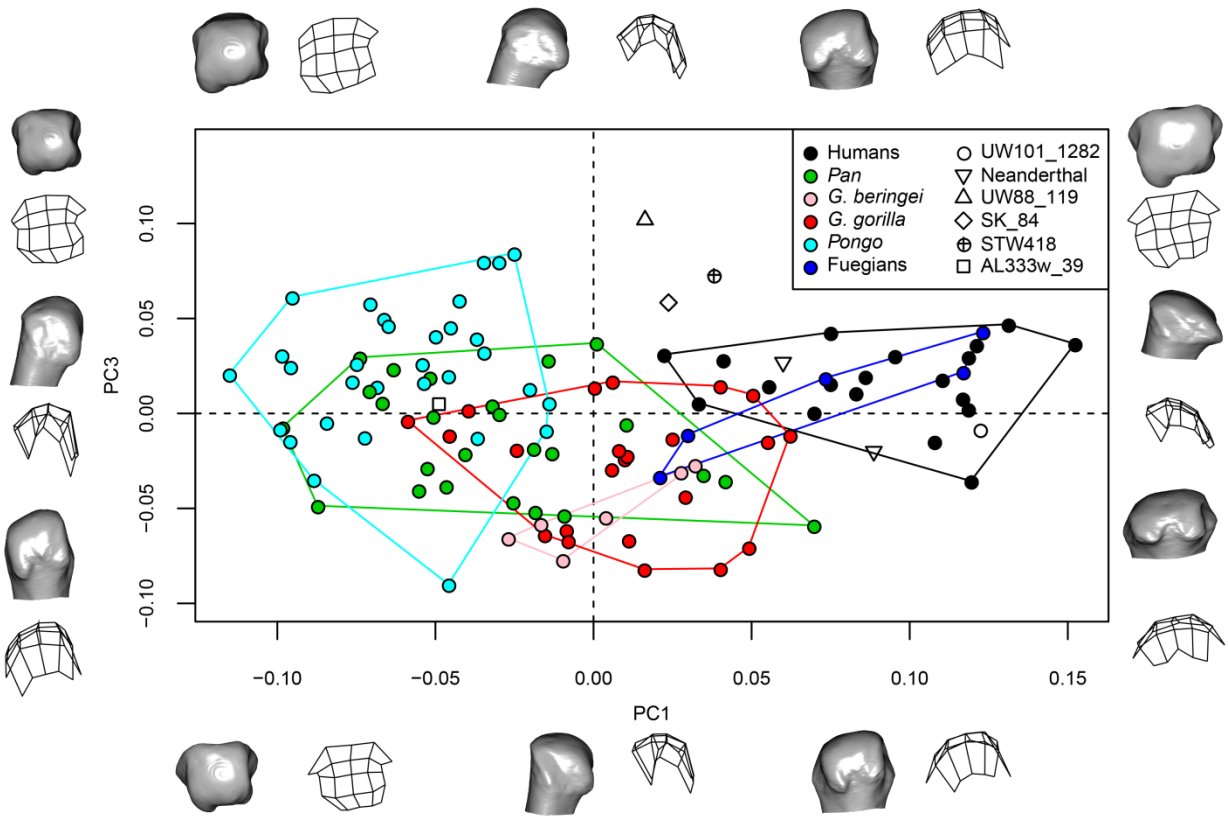

SOM Figure S8. Scatterplot of third vs. the second principal component (PC3 vs. PC1) scores of extant samples (non-Fuegian *Homo sapiens* labeled 'Humans' in figure, *H. sapiens* from Tierra del Fuego labeled 'Fuegians' in figure,, *Pan*, *Gorilla gorilla*, *Gorilla beringei*, and *Pongo*) and fossil specimens Tabun C1 and La Chapelle-aux-Saints (*Homo neanderthalensis* labelled Neanderthal in figure), U.W. 101-1282 (*Homo naledi*), U.W. 88-119 (*Australopithecus sediba*), SK 84 (*Paranthropus robustus*/*Homo erectus*), StW 418 (*Australopithecus africanus*) and A.L. 333w-39 (*Australopithecus afarensis*). The mesh/wireframes show extreme shape for each axis. For each mesh/wireframe, radial is on the left, dorsal is superiorly. Meshes/wireframes are shown from three different points of view, from top to bottom or from left to right: distal view, radial view, palmar view.

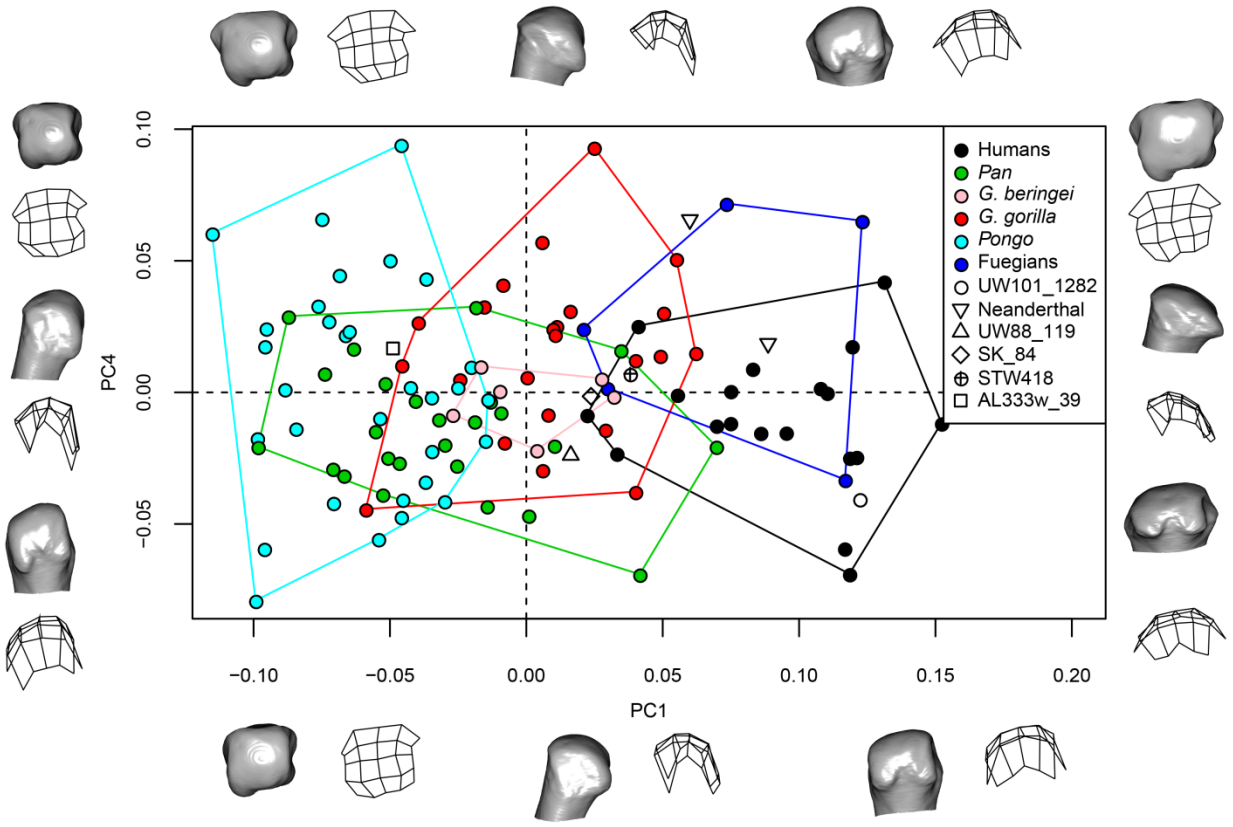

SOM Figure S9. Scatterplot of the fourth vs. the first principal component (PC4 vs. PC1) scores of extant samples (non-Fuegian *Homo sapiens* labeled 'Humans' in figure, *H. sapiens* from Tierra del Fuego labeled 'Fuegians' in figure, *Pan*, *Gorilla gorilla*, *Gorilla beringei*, and *Pongo*) and fossil specimens Tabun C1 and La Chapelle-aux-Saints (*Homo neanderthalensis*, labelled Neanderthal in figure), U.W. 101-1282 (*Homo naledi*), U.W. 88-119 (*Australopithecus sediba*), SK 84 (*Paranthropus robustus*/*Homo erectus*), StW 418 (*Australopithecus africanus*) and A.L. 333w-39 (*Australopithecus afarensis*). The mesh/wireframes show extreme shape for each axis. For each mesh/wireframe, radial is on the left, dorsal is superiorly. Meshes/wireframes are shown from three different points of view, from top to bottom or from left to right: distal view, radial view, palmar view.

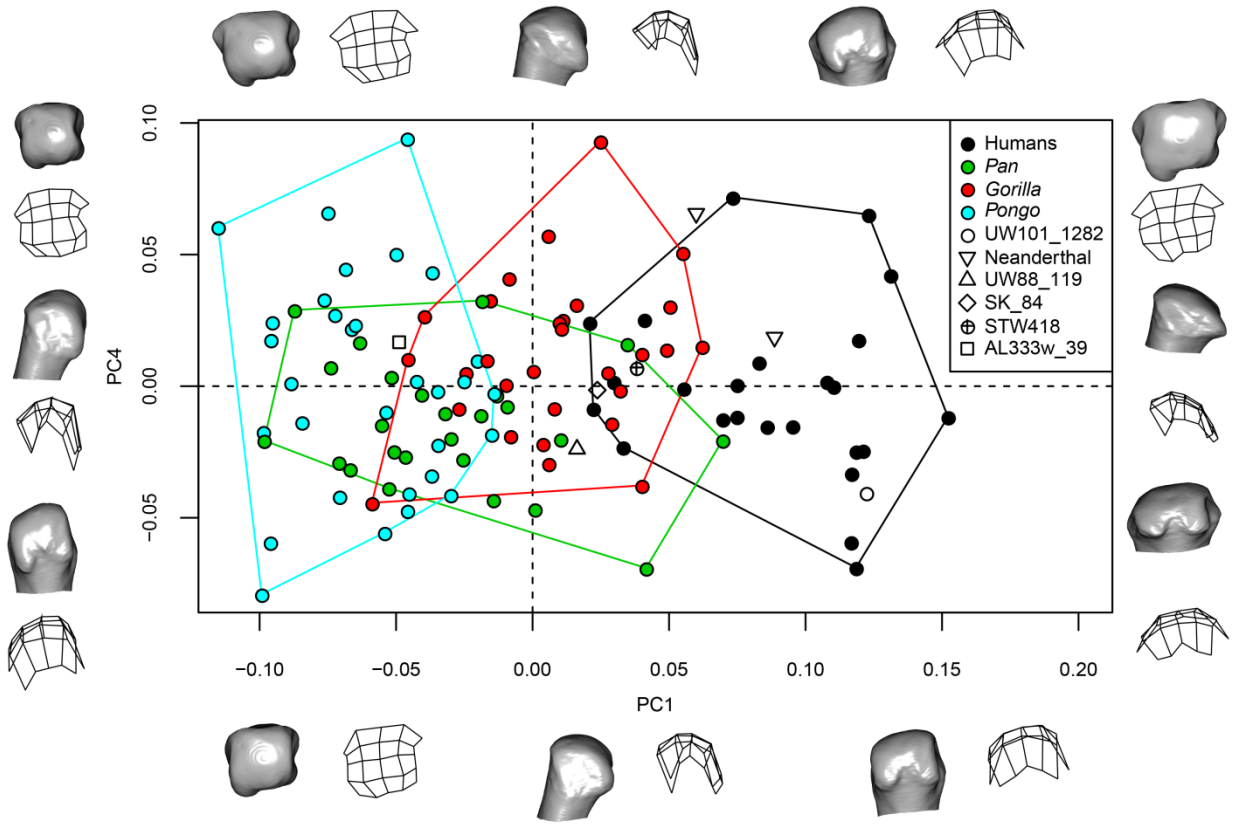

SOM Figure S10. Scatterplot of the fourth vs. the first principal component (PC4 vs. PC1) scores of extant samples (*Homo sapiens* labeled 'Humans' in figure, *Pan*, *Gorilla*, and *Pongo*) and fossil specimens Tabun C1 and La Chapelle-aux-Saints (*Homo neanderthalensis*, labelled Neanderthal in figure), U.W. 101-1282 (*Homo naledi*), U.W. 88-119 (*Australopithecus sediba*), SK 84 (*Paranthropus robustus*/early *Homo*), StW 418 (*Australopithecus africanus*) and A.L. 333w-39 (*Australopithecus afarensis*). The mesh/wireframes show extreme shape for each axis. For each mesh/wireframe, radial is on the left, dorsal is superiorly. Meshes/wireframes are shown from three different points of view, from top to bottom or from left to right: distal view, radial view, palmar view.

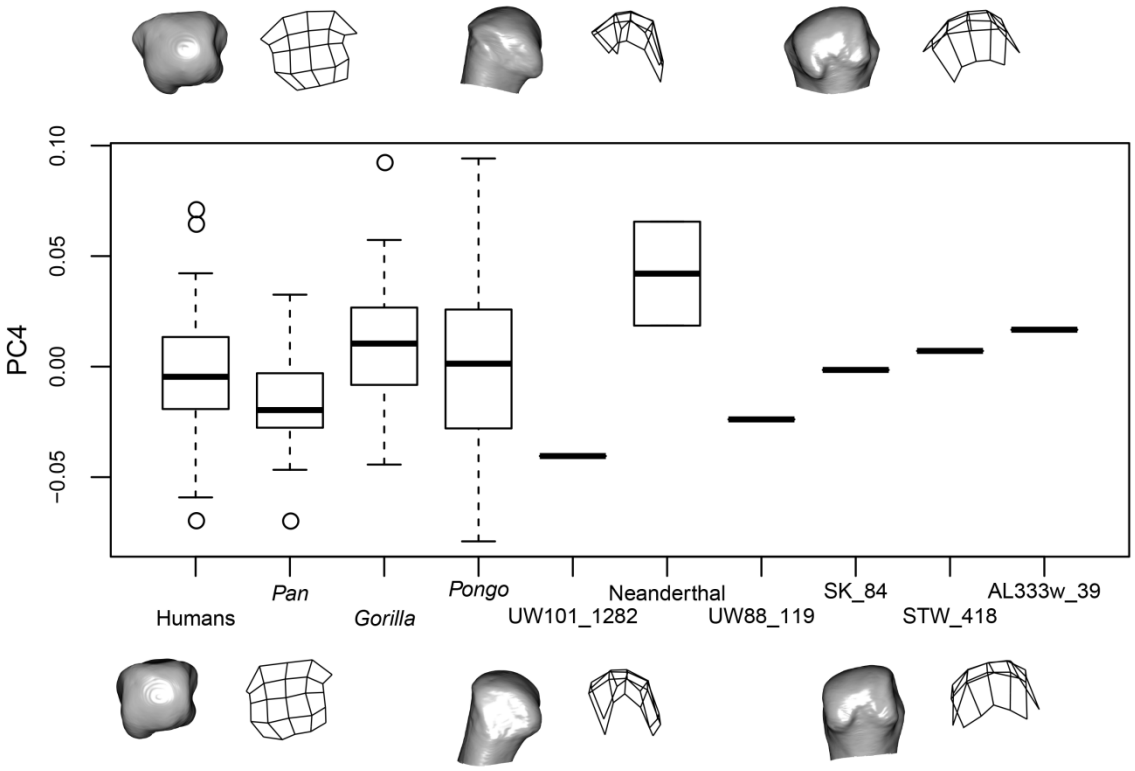

SOM Figure S11. Boxplot of the fourth principal component (PC4) scores for *Homo sapiens* (labeled 'Humans' in figure), *Pan*, *Gorilla* and *Pongo* compared to fossil specimens Tabun C1 and La Chapelle-aux-Saints (*Homo neanderthalensis*, labeled Neanderthal in figure), U.W. 101-1282 (*Homo naledi*), U.W. 88-119 (*Australopithecus sediba*), SK 84 (*Paranthropus robustus*/early *Homo*), StW 418 (*Australopithecus africanus*) and A.L. 333w-39 (*Australopithecus afarensis*). Black lines are the medians, boxes are the interquartile ranges, whiskers are the non-outlier ranges and empty circles are outliers.

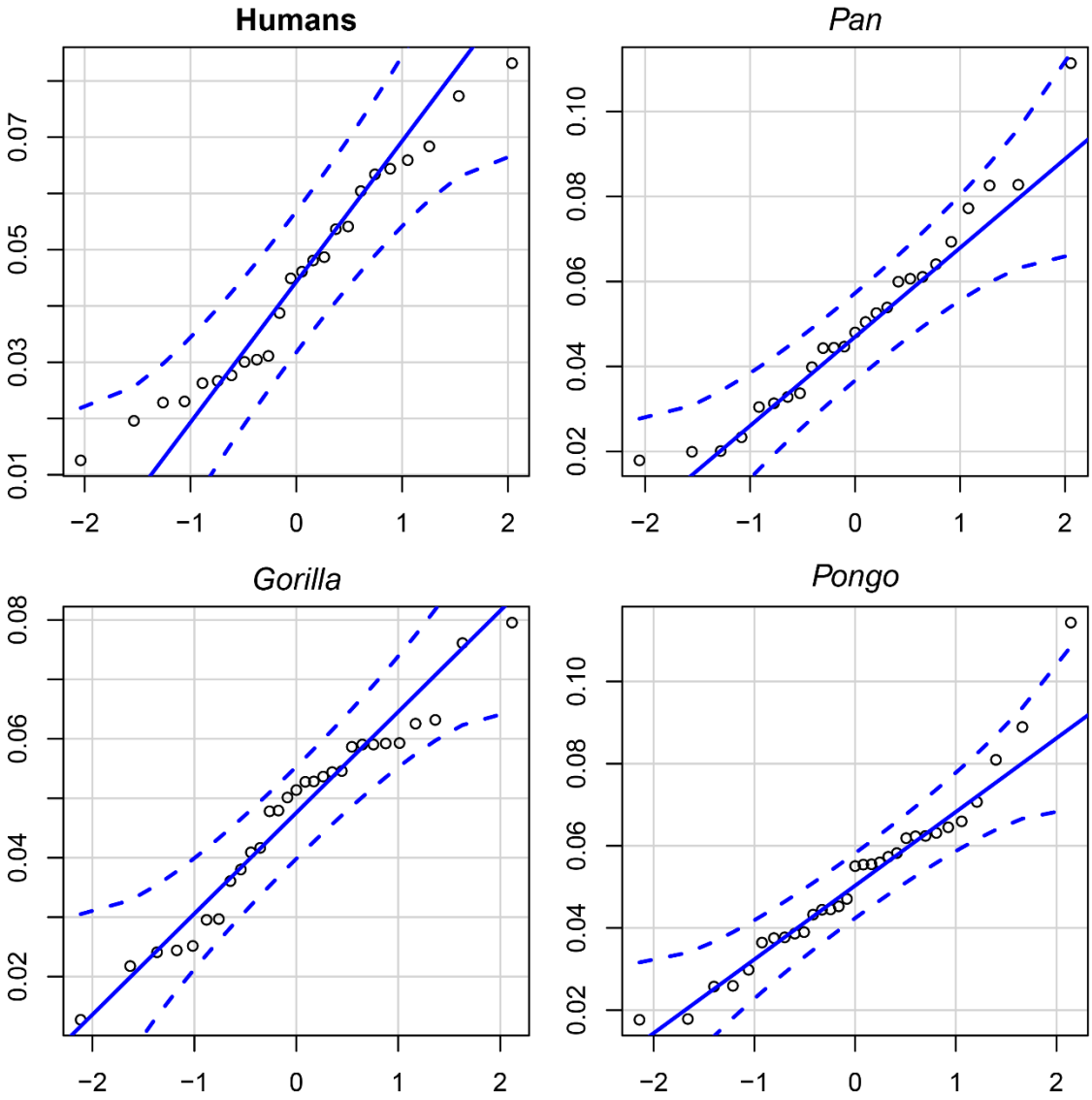

SOM Figure S12. Quantile-quantile (Q-Q-) plots of the distance of each individual within every extant group (modern humans, labeled 'Humans', *Pan*, *Gorilla* and *Pongo*) from the mean shape of the respective group.

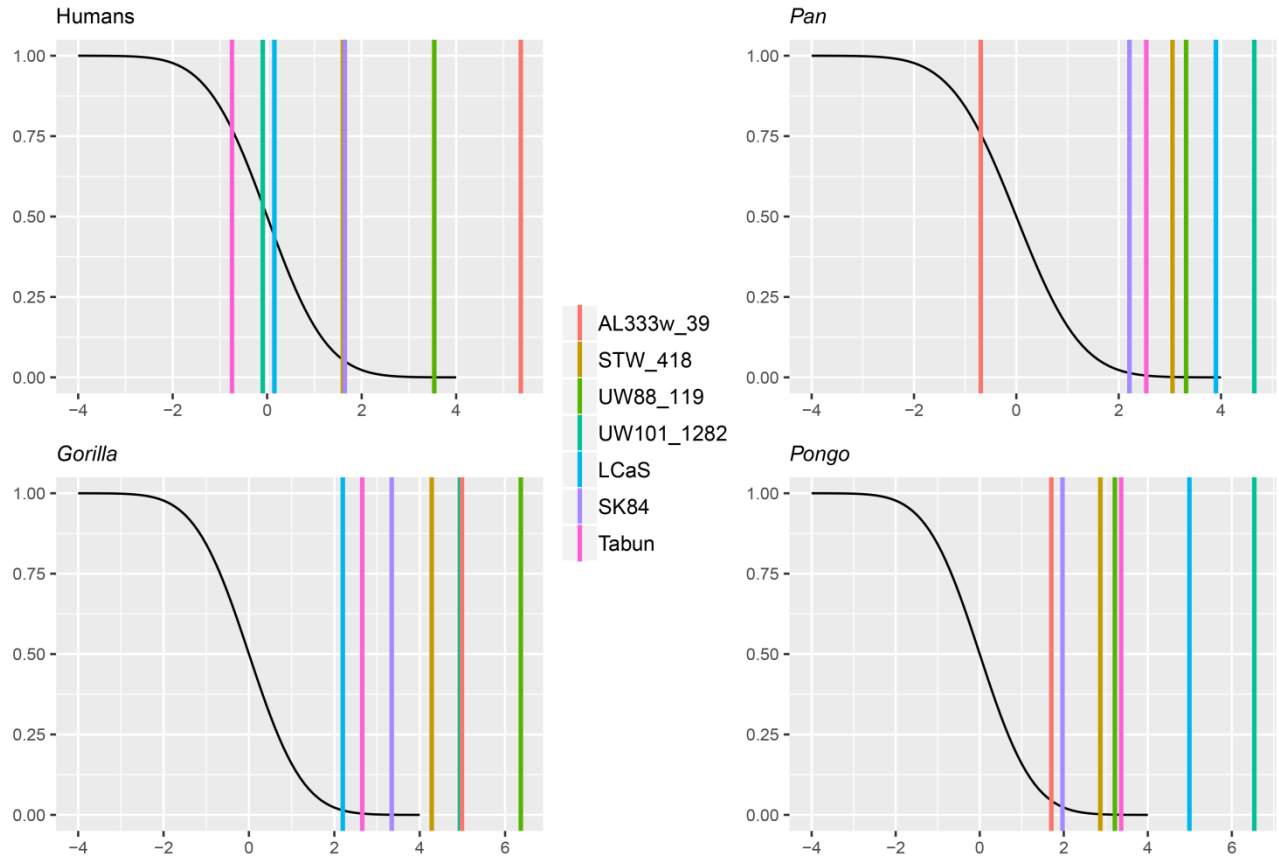

SOM Figure S13. Graphical representation of the distance (in standard deviations) of *Homo neanderthalensis* (Tabun C1, labelled Tabun and La Chapelle-aux-Saints, labelled LCaS) *Homo naledi* (U.W. 101-1282), *Australopithecus sediba* (U.W. 88-119), *Paranthropus robustus*/early *Homo* (SK 84), *Australopithecus africanus* (StW 418) and *Australopithecus afarensis* (A.L. 333w-39) from the mean of the distance of each individual of the extant groups (modern humans, labeled 'Humans', *Pan*, *Gorilla* and *Pongo*) from the group mean. On the horizontal axis is the distance in standard deviations from the mean distance. The black line is the upper tail cumulative distribution function (values on the orthogonal axis).

SOM Table S1

Comparison of results of regression analysis of principal component scores on ln(femoral superoinferior diameter) (FemSI) and log(centroid size) (CS). ln(FemSI) is the natural log transformed value of FemSI. ln(CS) is the natural log transformed value of the CS. The comparison has been carried on a subsample of the comparative sample. See text for details.

PC	ln(FemSI)		ln(CS)	
	Adjusted R^2	*p* value	Adjusted R^2	*p* value
PC1	0.32	< 0.00001	0.32	< 0.00001
PC2	0.04	0.11	0.06	0.06
PC3	0.13	0.01	0.10	0.03
PC4	0.02	0.21	0.01	0.24

SOM Table S2

MANCOVA analysis results. ‘x’ indicates independent variables crossing. ‘:’ indicates the interaction term of the full model. To estimate *p* values, we used the Pillai test statistic. ln(FemSI) is the natural log-transformed value of femoral superioinferior diameter. ln(CS) is the natural log-transformed value of centroid size. ‘Group’ is the categorical variable in which is divided the comparative sample (humans, *Pan, Gorilla, Pongo*).

Model[a]	Term	*p* value
ln(FemSI) x Group	ln(FemSI)	0.43
	Species	$p < 0.00001$
	ln(FemSI) : Group	0.74
ln(CS) x Group	ln(CS)	0.11
	Species	$p < 0.00001$
	ln(CS) : Group	0.08

[a] The two models have been applied to different subsamples of the extant sample. See text for details.

SOM Table S3

Repeatability test results expressed as *p*-values of the multivariate Levene test (Anderson in table)

Taxon	Anderson
Homo	< 0.01
Pan	< 0.01
Gorilla	< 0.01
Pongo	< 0.001

SOM Table S4

Results of the Hotelling's T^2 test on the first four principal components (sample size in parentheses).

Comparison	Modern humans (n = 19) – Fuegians (n = 5)	*Gorilla gorilla* (n = 23) – *Gorilla beringei* (n = 6)
p	0.15	0.29

SOM Table S5

Tukey honestly significant difference (HSD) post hoc test results on principal component 4 scores. In bold are significant results ($p < 0.05$).

Group		Mean difference	*p*	95% confidence interval	
				Lower bound	Upper bound
Homo	*Pan*	0.012	0.547	-0.012	0.037
	Gorilla	-0.013	0.450	-0.037	0.010
	Pongo	-0.003	0.983	-0.027	0.020
Pan	*Homo*	-0.012	0.547	-0.037	0.012
	Gorilla	-0.026	**0.024**	-0.049	-0.003
	Pongo	-0.016	0.286	-0.039	0.007
Gorilla	*Homo*	0.013	0.450	-0.010	0.037
	Pan	0.026	**0.024**	0.003	0.049
	Pongo	0.010	0.630	-0.012	0.032
Pongo	*Homo*	0.003	0.983	-0.020	0.027
	Pan	0.016	0.286	-0.007	0.039
	Gorilla	-0.010	0.630	-0.032	0.012

Table 1

Sample composition.

Taxon	*n* / fossil ID	Institution	Sex			Side	
			Male	Female	Unknown	Right	Left
Extant							
Homo sapiens	19	SACM, MHP	10	9	—	6	13
Fuegians	5	UF	2	—	3	1	4
Pan troglodytes	25	SCZ, SZCM, NMS, MPITC,PCM	11	14	4	12	13
Gorilla gorilla	23	SCZ, SZCM, PCM, PCZ, ZMB	11	11	1	13	10
Gorilla beringei	6	NMNH, RMCA	3	3	—	1	5
Pongo abelii	5	PCZ, NMS, ZMB, NML, NMNH	2	3	—	5	—
Pongo pygmaeus	26	SCZ, SZCM, PCZ, ZMB, NMS	10	15	1	14	12
Fossils							
Homo neanderthalensis	Tabun C1	NHML	—	—	—	—	1
	La Chapelle aux Saints	MHP	—	—	—	1	—
Homo naledi	U.W. 101-1282	WITS	—	—	—	—	1
Australopithecus sediba	U.W. 88-119	WITS	—	1	—	1	—
Paranthropus robustus/early *Homo*	SK 84	Ditsong	—	—	—	—	1
Australopithecus	StW 418	WITS	—	—	—	1	—

africanus						
Australopithecus afarensis	A.L. 333w-39	—	—	—	1	—

Abbreviations: Ditsong = Ditsong Museum, Pretoria, South Africa; MHP = Musée de l'Homme, Paris, France; MPITC = Max Plank Institute, Tai Collection, Leipzig, Germany; NHML = Natural History Museum, London, UK; NML = Naturalis Museum, Leiden, Netherlands; NMNH = Smithsonian, National Museum of Natural History, Washington, USA; NMS = Naturmuseum Senckenberg, Frankfurt, Germany; PCM = Powel Cotton Museum, Birchington, UK; PCZ = Primate Collection, Zürich, Switzerland; RMCA = Royal Museum for Central Africa, Tervuren, Belgium; SACM = State Anthropological Collection, Münich, Germany; SCZ = Shultz Collection, University of Zürich Irchel, Switzerland; SZCM = State Zoological Collection, Münich, Germany; UF = University of Florence Anthropological Collection, Florence, Italy; WITS = Evolutionary Studies Institute, University of the Witwatersrand, South Africa; ZMB = Zoologisches Museum Berlin, Germany.

Table 2

Definitions of the 9 fixed landmarks.

No	Definition	Type
1	Most proximal point on the palmar-radial condyle	2
2	Midpoint between points 1 and 3 on the palmar articular ridge	3
3	Most proximal point on the palmar-ulnar condyle	2
4	Projection of point 5 on the lateral ridge of the articulation	3
5	Central point of the distal articulation	3
6	Projection of point 5 on the medial ridge of the articulation	3
7	Most lateral point on the radial epicondyle	2
8	Projection of point 1 on the dorsal ridge of the articulation	3
9	Most medial point on the ulnar epicondyle	2

Table 3

Tukey honestly significant difference (HSD) post hoc test results on principal component 1 scores. In bold are significant results ($p < 0.05$).

Group		Mean difference	*p*	95% confidence interval	
				Lower bound	Upper bound
Homo	*Pan*	0.118	**<0.001**	0.092	0.143
	Gorilla	0.079	**<0.001**	0.055	0.104
	Pongo	0.147	**<0.001**	0.123	0.171
Pan	*Homo*	-0.118	**<0.001**	-0.143	-0.092
	Gorilla	-0.038	**<0.001**	-0.063	-0.014
	Pongo	0.029	**0.010**	0.005	0.053
Gorilla	*Homo*	-0.079	**<0.001**	-0.104	-0.055
	Pan	0.038	**<0.001**	0.014	0.063
	Pongo	0.068	**<0.001**	0.045	0.091
Pongo	*Homo*	-0.147	**<0.001**	-0.171	-0.123
	Pan	-0.029	**0.010**	-0.053	-0.005
	Gorilla	-0.068	**<0.001**	-0.091	-0.045

Table 4

Tukey honestly significant difference (HSD) post hoc test results on principal component 2 scores. In bold are significant results ($p < 0.05$).

Group		Mean difference	p	95% confidence interval	
				Lower bound	Upper bound
Homo	*Pan*	-0.041	**<0.001**	-0.061	-0.020
	Gorilla	0.047	**<0.001**	0.027	0.067
	Pongo	0.022	**0.023**	0.002	0.041
Pan	*Homo*	0.041	**<0.001**	0.020	0.061
	Gorilla	0.088	**<0.001**	0.068	0.107
	Pongo	0.06	**<0.001**	0.043	0.081
Gorilla	*Homo*	-0.047	**<0.001**	-0.067	-0.027
	Pan	-0.088	**<0.001**	-0.107	-0.068
	Pongo	-0.025	**0.003**	-0.044	0.007
Pongo	*Homo*	-0.022	**0.023**	-0.041	-0.002
	Pan	-0.06	**<0.001**	-0.081	-0.043
	Gorilla	-0.088	**0.003**	-0.107	-0.068

Table 5

Tukey honestly significant difference (HSD) post hoc test results on principal component 3 scores. In bold are significant results ($p < 0.05$).

Group		Mean difference	*p*	95% confidence interval	
				Lower bound	Upper bound
Homo	*Pan*	0.029	**0.007**	0.006	0.052
	Gorilla	0.048	**<0.001**	0.026	0.071
	Pongo	-0.007	0.804	-0.029	0.014
Pan	*Homo*	-0.029	**0.007**	-0.052	-0.006
	Gorilla	0.019	0.109	-0.003	0.041
	Pongo	-0.037	**<0.001**	-0.058	-0.014
Gorilla	*Homo*	-0.048	**<0.001**	-0.071	-0.026
	Pan	-0.019	0.109	-0.041	0.003
	Pongo	-0.056	**<0.001**	-0.077	-0.035
Pongo	*Homo*	0.007	0.804	-0.014	0.029
	Pan	0.037	**<0.001**	0.014	0.058
	Gorilla	0.029	**<0.001**	0.035	0.077

Table 6

Mean and standard deviation (within parentheses) of principal component (PC) scores for *Homo*, *Pan*, *Gorilla*, and *Pongo* compared with PC scores of fossil specimens Tabun C1 and La Chapelle-aux-Saints (*Homo neanderthalensis*), U.W. 101-1282 (*Homo naledi*), U.W. 88-119 (*Australopithecus sediba*), SK 84 (*Paranthropus robustus*/early *Homo*), StW 418 (*Australopithecus africanus*) and AL 333w-39 (*Australopithecus afarensis*). [a]

Group	*Homo*	*Pan*	*Gorilla*	*Pongo*	Tabun C1	La Chapelle-aux-Saints	U.W. 101-1282	U.W. 88-119	SK 84	StW 418	AL 333w-39
	(*n* = 24)	(*n* = 25)	(*n* = 29)	(*n* = 31)							
PC1	0.087	-0.031	0.008	-0.060	$0.060_{P,G,Po}$	$0.089_{P,G,Po}$	$0.122_{P,G,Po}$	$0.016_{H,P,Po}$	$0.023_{H,P,Po}$	$0.038_{H,P,Po}$	$-0.049_{H,G}$
	(0.038)	(0.041)	(0.031)	(0.028)							
PC2	0.008	0.049	-0.039	-0.013	$0.005_{P,G}$	$-0.023_{H,P}$	$0.014_{P,G}$	$0.031_{H,G,Po}$	$-0.004_{P,G}$	$0.002_{P,G}$	$0.071_{H,G,Po}$
	(0.023)	(0.026)	(0.025)	(0.033)							
PC3	0.015	-0.014	-0.033	0.023	$0.027_{P,G}$	$-0.020_{H,Po}$	-0.008_{H}	$0.102_{H,P,G,Po}$	$0.058_{H,P,G}$	$0.073_{H,P,G,Po}$	0.005_{G}
	(0.022)	(0.029)	(0.031)	(0.037)							
PC4	-0.002	-0.014	0.011	0.001	$0.066_{H,P,G,Po}$	0.019_{P}	$-0.040_{H,P,G,Po}$	-0.024_{P}	0.001	0.007	0.017_{P}
	(0.033)	(0.024)	(0.029)	(0.041)							

[a] Subscripts indicate which group differs at least 1 SD from the fossils. Abbreviations: H = *H. sapiens*, P = *Pan*, G = *Gorilla*, Po = *Pongo*.

Table 7

Discriminant function analysis (DFA) classification results of fossil specimens.

	Homo sapiens	*Pan*	*Gorilla*	*Pongo*
Tabun C1	97.5%	0.8%	1.4%	0.3%
La Chapelle-aux-Saints	76.6%	0.0%	23.4%	0.0%
U.W. 101-1282	99.9%	0.0%	0.1%	0.0%
U.W. 88-119	29.7%	32.0%	0.0%	38.4%
SK 84	59.1%	11.9%	1.2%	27.8%
StW 418	88.6%	2.8%	0.4%	8.2%
AL 333w-39	0.0%	97.8%	0.0%	2.2%

Table 8

Results of the Shapiro-Wilk normality test performed on the individual distances distribution from their respective group mean shape. Calculations have been done on linear distances considering the principal components 1–3.

	Homo sapiens	*Pan*	*Gorilla*	*Pongo*
p	0.35	0.30	0.33	0.15

Table 9

Fossils distances in standard deviations from the mean distance of extant groups from theirs' mean shape. In parentheses, the value of the upper tail cumulative distribution function multiplied by 100 Fossils distances in standard deviations from the mean distance of extant groups from theirs mean shape. Calculations have been done on linear distances considering the first principal components 1–3.

	Homo sapiens	*Pan*	*Gorilla*	*Pongo*
Tabun C1	-0.74 (77.2%)	2.54 (0.55%)	2.65 (0.40%)	3.37 (0.04%)
La Chapelle-aux-Saints	0.15 (43.9%)	3.90 (0.00%)	2.20 (1.40%)	4.99 (0.00%)
U.W. 101-1282	-0.09 (53.7%)	4.65 (0.00%)	4.94 (0.00%)	6.53 (0.00%)
U.W. 88-119	3.54 (0.02%)	3.32 (0.05%)	6.37 (0.00%)	3.22 (0.06%)
SK 84	1.64 (5.01%)	2.21 (1.35%)	3.34 (0.04%)	1.97 (2.45%)
StW 418	1.60 (5.46%)	3.05 (0.11%)	4.28 (0.00%)	2.87 (0.21%)
AL 333w-39	5.37 (0.00%)	-0.69 (75.7%)	4.99 (0.00%)	1.70 (4.42%)